



Would delineation of nitrate vulnerable zones be improved by introducing a new parameter representing the risk associated with soil permeability in the Land Use–Intrinsic Vulnerability Procedure?

Mercedes Arauzo^{a,*}, María Valladolid^b, Delia M. Andries^c

^a Instituto de Ciencias Agrarias (ICA), CSIC, Serrano 115 dpdo, 28006 Madrid, Spain

^b Museo Nacional de Ciencias Naturales (MNCN), CSIC, José Gutiérrez Abascal 2, 28006 Madrid, Spain

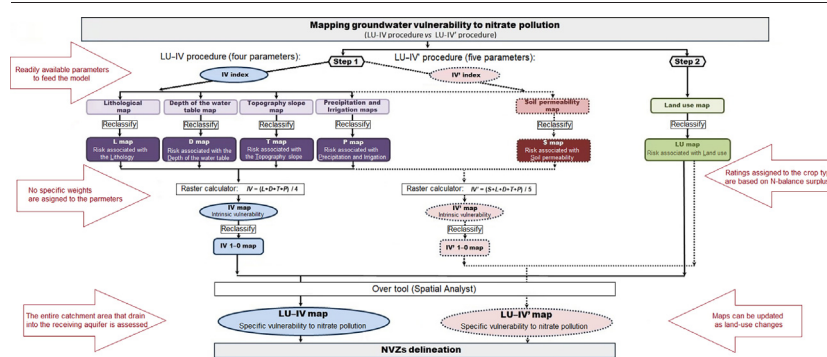
^c Facultad de Ciencias Geológicas, Universidad Complutense de Madrid, José Antonio Novais 12, 28040 Madrid, Spain



HIGHLIGHTS

- The LU–IV procedure considers the solute transport through the aquifer catchment area.
- Models that used the LU–IV procedure were the best predictors of nitrate pollution.
- Including a soil parameter in the LU–IV procedure was unnecessary for good results.
- The LU–IV procedure was the best and simplest method of those tested to delimit NVZs.
- The LU–IV procedure identified twice the area of the designated NVZs as designable.

GRAPHICAL ABSTRACT



ARTICLE INFO

Editor: Christian Herrera

Keywords:

Specific groundwater vulnerability to nitrate pollution

Intrinsic groundwater vulnerability
Geographic Information System (GIS)

ABSTRACT

Most methods for mapping groundwater vulnerability are based on the excessively simplistic approach that aquifer recharge is produced by vertical infiltration. The novel Land Use–Intrinsic Vulnerability (LU–IV) procedure assesses groundwater vulnerability to nitrate pollution over the entire territory, including aquifers catchment areas. In this research, it was analysed if the delineation of nitrate vulnerable zones (NVZs) would be improved by introducing a new parameter representing the risk associated with soil permeability (parameter S) in the procedure. Different versions of parameter S were tested: S_{HC} (risk associated with soil hydraulic conductivity), S_{St + G + S} (risk associated with the stone, gravel and sand fraction of the soil) and S_C (risk associated with the clay fraction). The study was undertaken in the catchment areas of the Oja and Tirón alluvial aquifers (Spain). The efficacy of the following six models was compared: Model 1 (original LU–IV procedure), Model 2 (LU–IV' procedure using parameter S_{HC}), Model 3 (LU–IV' procedure using parameter S_{St + G + S}), Model 4 (LU–IV' procedure using parameter S_C), Model 5 (LU–DRASTIC–COP procedure, based on DRASTIC–COP method), and Model 6 (designated NVZ). Catchment scale validations of the six models showed similar, highly significant correlations between the percent coverages of the estimated NVZs and those of the alluvial areas polluted by nitrate for Models 1 to 4. Models 5 and 6 did not show any significant results. In light of these results, Models 1 to 4 were considered the best predictors of nitrate pollution and the best methods for NVZ delineation. Results support the idea that including a parameter S in the LU–IV' procedure is not essential since equivalent results were obtained from the original LU–IV procedure. So, the LU–IV procedure should be considered the best and simplest method of those tested for accurately delineating NVZs.

* Corresponding author at: Diffuse Pollution Group, Soil, Plant and Environmental Quality Department, Institute of Agricultural Sciences (ICA), Spanish National Research Council (CSIC); Serrano 115bis, 28006 Madrid, Spain.

E-mail address: mercedes.arauzo@csic.es (M. Arauzo).

1. Introduction

The Nitrates Directive of the European Union (91/676/EEC; Council of the European Communities, 1991) aims to reduce and prevent water pollution caused by nitrates from agricultural sources. It establishes that water resources should be considered polluted when nitrate concentration exceeds 50 mg L^{-1} . The Directive requires the Member States to designate nitrate vulnerable zones (NVZs), which are areas that drain into waters polluted or at risk of pollution by nitrates. In NVZs, farmers must follow mandatory measures within action programmes that include limiting N-fertilization and animal manure application to prevent nitrate leaching and runoff.

One of the difficulties in implementing the European environmental policies for nitrate pollution control is the lack of a common standard criterion for NVZ designation (European Commission, 2018). Several studies suggest that poorly delineated NVZs seriously compromise the effectiveness of action programs to reduce nitrate pollution (Arauzo and Martínez-Bastida, 2015; Arauzo et al., 2011; Orellana-Macías et al., 2020; Richard et al., 2018; Worrall et al., 2009). It is therefore necessary to improve accuracy in NVZ designations in order to maximise the effectiveness of the action programmes (European Commission, 2018; Arqued, 2018).

Index-based groundwater vulnerability mapping has proven to be useful tools to assist governments in establishing policies related to the planning of water resource management over the last few decades, but there are still research gaps related to risk mapping, assessment techniques and scientific considerations behind the inclusion/exclusion of parameters and the relative ratings and weights assigned to the parameters (Kumar et al., 2015). Debernardi et al. (2008) and Stigter et al. (2006) expressed doubts about the reliability of groundwater vulnerability mapping models due to the discrepancies that can be observed between the vulnerability maps and the nitrate pollution maps. Arauzo (2017), Arauzo and Martínez-Bastida (2015), and Zahid et al. (2015) attributed such discrepancies to long-distance nitrate displacement by advective transport from the highest to lowest catchment areas, in addition to the accumulation/dilution processes within the saturated zone. Hrachowitz et al. (2016) pointed out the importance of hydrology-controlled transport through catchment systems as the link between hydrology and water quality (whose models are still relatively disconnected in spite of trying to understand processes in the same spatial domain). In this sense, Machiwal et al. (2018) suggested the need for developing robust and versatile methodologies for assessing the intrinsic and specific vulnerability of groundwater under varying hydrogeologic and hydroclimatic conditions, using a 'source-pathway-receptor' approach that involves modelling at the catchment scale (intrinsic vulnerability is based on an assessment of natural climatic, geological and hydrogeological attributes, whereas specific vulnerability is mainly assessed in terms of the risk of the groundwater system becoming exposed to contaminant loading; Witkowski et al., 2007). Likewise, Nadiri et al. (2018a, 2018b) adopted the innovative OSPRC (Origins, Sources, Pathways, Receptors, Consequences) framework to integrate information for indexing risks to aquifers exposed to diffuse pollution.

The LU-IV procedure (land use-intrinsic vulnerability procedure; Arauzo, 2017; Arauzo et al., 2019, 2020; Fig. 1) was developed to address the above-stated challenges. It allows assessing the intrinsic vulnerability of groundwater and its specific vulnerability to nitrate pollution over the entire surface of the territory (including aquifers catchment areas) and, where necessary, the accurate delineation of the NVZs. The procedure combines a map of intrinsic vulnerability (IV map), based on the IV index (Arauzo, 2017), and a map of the risk of N-loss associated with land use (LU map) by applying the Logical Math tools in ArcGIS 10.3 (ESRI, 2015), to generate the map of vulnerability to nitrate pollution (LU-IV map). The LU-IV map assesses the risk of nitrate leaching associated with land use in intrinsically vulnerable territories by analysing not just the aquifer surface but rather the entire surface of the territory. This recent methodology has the following differential characteristics: (1) it uses readily available parameters to feed the model, (2) it does not assign specific weights to the parameters, (3) it allows assessing the entire catchment area that

drains into the aquifer, (4) it permits periodical map updating as land use changes over time, and (5) the ratings assigned to the crop types in the LU map are fine-tuned using empirical data on the N-balance surpluses in agriculture (Arauzo et al., 2019).

The IV index (step 1 of the LU-IV procedure; Fig. 1) evaluates the intrinsic vulnerability from four environmental parameters that, in turn, assess the risks associated with the lithology of the vadose zone (parameter L), the depth of the water table (parameter D), the topography slope (parameter T) and the precipitation and irrigation (parameter P). This index proved to be more accurate than the most widely used intrinsic vulnerability indices DRASTIC (Aller et al., 1987) and GOD (Foster et al., 2002), having been tested on the catchment areas of 46 groundwater masses in the Ebro River basin (Spain; Arauzo, 2017). Despite this, its algorithm does not include a parameter for evaluating the risk associated with soil permeability. Soil permeability, however, has a significant impact on the amount of recharge that can infiltrate into the ground and hence on the ability of solutes to move into the vadose zone (Aller et al., 1987; Arauzo et al., 2022; Witkowski et al., 2007). Water flow is induced by gravity and the cohesive and adhesive forces set up in the soil. The rate of flow in unsaturated soils is a complex function of the size, shape and distribution of the pores and fissures, the soil chemistry and the presence of air. Soils with large pores drain easily. Silt and clay soils have small pores and retain water, while clays that expand when wet may become impermeable (Franceys et al., 1992). Clay also plays a regulatory role in nitrate availability in the soil solution (Arauzo et al., 2022). It would, therefore, be necessary to analyse to what extent the delineation of NVZs would improve if a new parameter evaluating the risk associated with soil permeability is included in the IV index of the procedure. However, on the other hand, the generally scarce availability of soil permeability georeferenced data to adequately feed this type of model could affect the robustness of the intrinsic vulnerability maps, which could pose a significant limitation.

In this research, it was analysed whether the assessment of groundwater vulnerability to nitrate pollution and the delineation of NVZs would significantly improve by including information on the soil permeability in the IV index of the LU-IV procedure. To that aim, a fifth parameter was added to the IV index, representing the risk associated with soil permeability (parameter S). Thus a new intrinsic vulnerability index was generated, the IV' index, which constitutes step 1 of the new LU-IV' procedure (Fig. 1). As there are different parameters directly related to soil permeability and percolating capacity of solutes, three of them that are easily estimable were selected to be tested as parameter S: the risk associated with the soil hydraulic conductivity (parameter S_HC), the risk associated with the stone, gravel and sand fraction of the soil (parameter S_St + G + S), and the risk associated with the clay fraction (parameter S_C). The main objective was to compare the efficacy of six different parametric models for assessing groundwater vulnerability to nitrate pollution and delineating potential NVZs. The models tested were as follows: Model 1 (original LU-IV procedure; Arauzo, 2017; Arauzo et al., 2019, 2020), Model 2 (LU-IV' procedure using the parameter S_HC), Model 3 (LU-IV' procedure using the parameter S_St + G + S), Model 4 (LU-IV' procedure using the parameter S_C), Model 5 (LU-DRASTIC-COP procedure), and Model 6 (NVZs officially designated in the area). The six models are described in Section 2.4, but it is advanced here that Model 5 uses the DRASTIC index (Aller et al., 1987) and the COP index (Vías et al., 2006) to generate the map of intrinsic vulnerability (IGME, 2009a, 2009b). The efficacy of the intrinsic vulnerability indices used in Models 1 to 5 to estimate NVZs was also explored.

2. Material and methods

2.1. Study area

The study area comprises the catchment areas that drain into the Oja Alluvial Aquifer and the Tirón Alluvial Aquifer (Fig. 2), located on the right bank of the upper Ebro River basin (north of Spain). The territory depends on the Spanish regions of La Rioja and Castilla y León. It covers a total surface area of 1397 km^2 for which the general climate is continental-

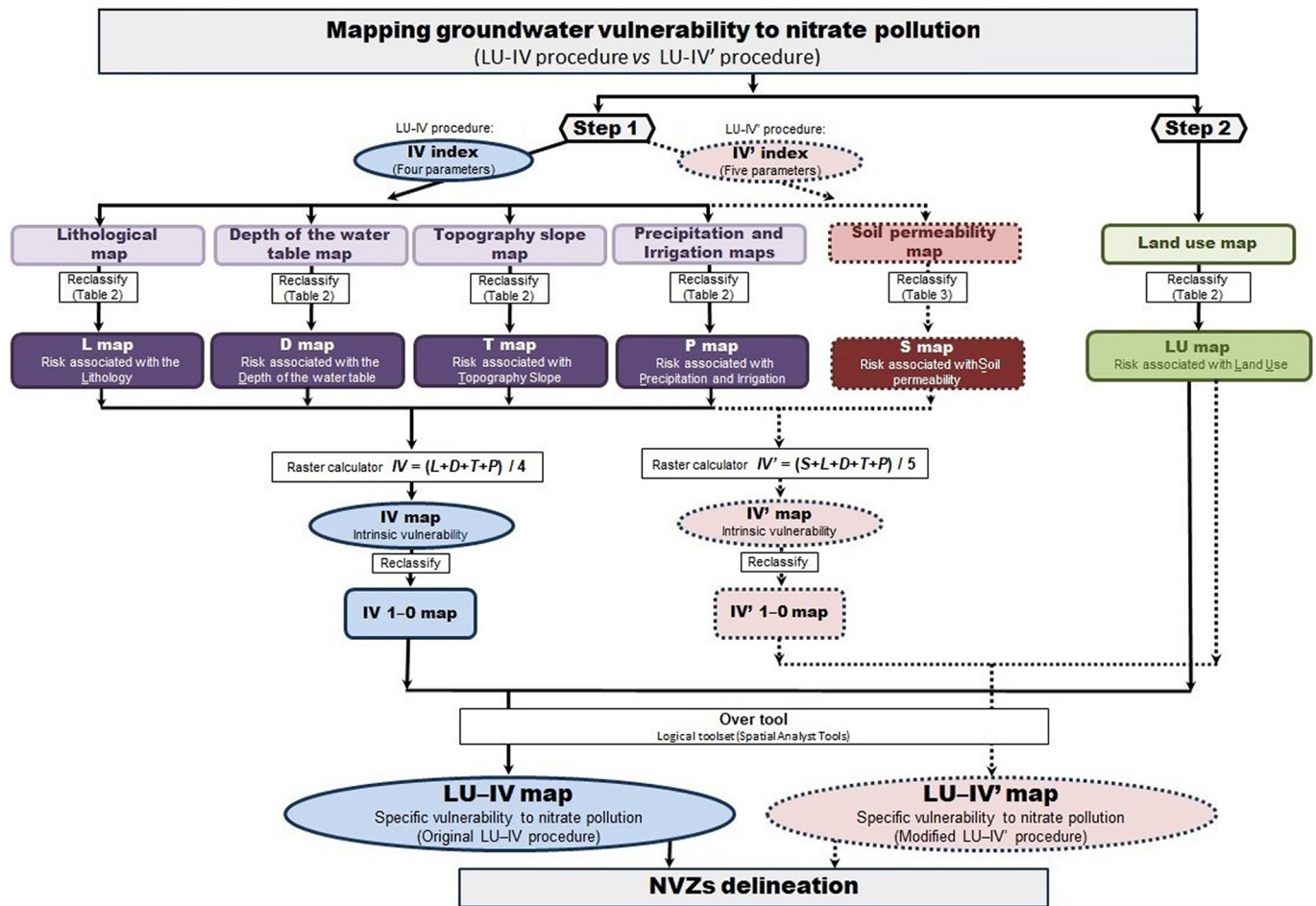


Fig. 1. Flow chart showing the original LU-IV procedure (with four parameters that make up the IV index; Arauzo, 2017) and the modified LU-IV' procedure (with five parameters that make up the index IV' through the inclusion of parameter S).

Mediterranean, although a mountain climate dominates in the highest areas.

Recharge of the Oja and Tirón aquifers depends on the infiltration from precipitation and irrigation returns from their respective catchment areas. Discharge occurs toward the rivers and by pumping extractions. The Oja aquifer is hydraulically linked to the Oja and Tirón rivers and the Zamaca and Valpierre streams (Fig. 2). The Tirón aquifer is hydraulically linked to the mid-upper reaches of the River Tirón (Fig. 2). The Oja and Tirón rivers meet together 9 km before draining into the River Ebro. The Zamaca and Valpierre streams are minor tributaries of the River Ebro and remain permanently dry in their mid-upper sections. The two aquifers are chronically affected by nitrate pollution (Arauzo et al., 2022). Their main characteristics are shown in Table 1. Besides nitrate pollution, the Oja aquifer is strongly affected by groundwater over-extraction during spring-summer irrigations (Arauzo et al., 2011). Agricultural land is widespread in the area, while forests and natural areas are maintained in the headwater areas. As a whole, the fluvial-alluvial system discharges into the River Ebro a water volume of about 240 hm³ year⁻¹ and a nitrogen load of about 2.4 kt year⁻¹ (Arauzo et al., 2011).

Maps of lithology, topography slope, mean annual precipitation and land use are shown in Fig. 3A, C, D and E. The prevailing soil types are cambisols, regosols and fluvisols, mostly with slightly alkaline pH (7.2 to 7.9) except at the headwaters of the Oja and Tirón rivers (4.1 to 5.9) (Arauzo et al., 2022). N contribution from municipal and industrial sewage is not significant since wastewater is channelled to a treatment plant that discharges into the River Ebro, outside the study area (Gobierno de La Rioja, 2010), which made it easier to focus on N from diffuse sources.

To date, an area of 94 km² has been designated as NVZ on the Oja aquifer (Gobierno de la Rioja, 2006a; Fig. 2 and Table 2). This area coincides with the most polluted zones of the aquifer (Arauzo et al., 2011), suggesting that nitrate concentration in groundwater was probably the criterion for the designation. No designations have been made in the Tirón aquifer so far.

2.2. Soil sampling, analysis and mapping

Soil sampling was carried out during April and May 2017. Soil samples were collected at 259 sampling points (Fig. 3F, G and H) through stratified sampling based on the soil types (Guerra et al., 1970; Fortalez et al., 1987). Two replicated samples were collected at each sampling point at a depth of 0–20 cm, obtaining a total of 518 soil samples. Depending on the abundance of coarse elements, 3–10 kg was collected per sample.

Two *in situ* measurements of soil hydraulic conductivity (K) were performed at the surface of each soil sampling point using a hand-held tension Mini Disk Infiltrometer (Decagon Devices, Pullman Washington, USA; Decagon Devices Inc., 2016). The Mini Disk Infiltrometer measures the unsaturated hydraulic conductivity at different applied tensions (adjustable suction from 0.5 to 7 cm). Infiltrating water under a tension prevents the filling of the macropores and gives a hydraulic conductivity characteristic of the soil matrix that is less spatially variable (Everst and Kanwar, 1993).

Granulometric analysis was performed on the 518 soil samples. The most common subdivision of soil granulometry into classes is the fine-earth fraction (clay, silt and sand) and the coarse fraction (gravel and stones). According to this classification, the following particle size fractions were measured on the soil samples: clay ($\phi \leq 0.002$ mm), silt ($0.002 \leq \phi <$

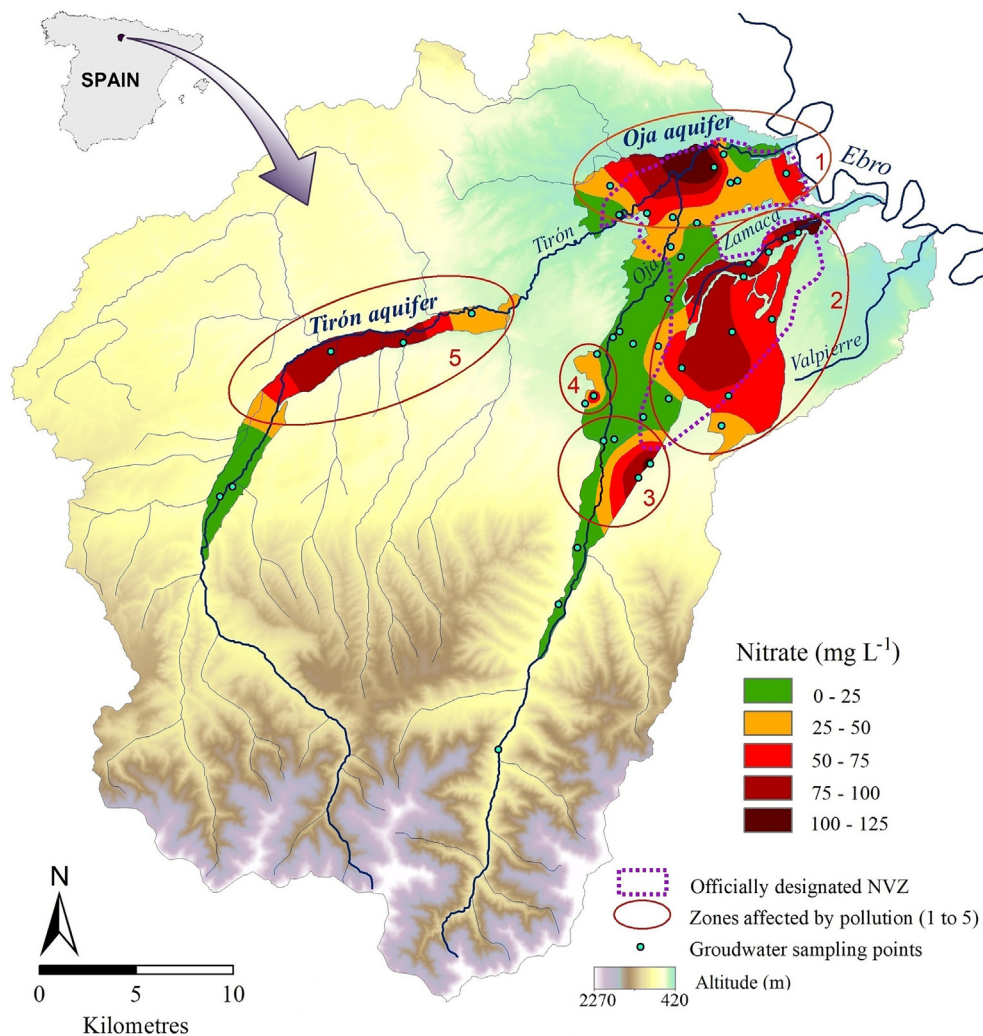


Fig. 2. Study area, which includes the Oja Alluvial Aquifer, the Tirón Alluvial Aquifer and their catchment areas (north of Spain). The mean nitrate concentration in groundwater during 2017, the location of groundwater sampling points and the designated NVZ (Gobierno de La Rioja, 2006a) are shown. The five zones affected by nitrate pollution are circled in red.

0.02 mm), sand ($0.02 \leq \phi < 2$ mm), gravel ($2 \leq \phi < 60$ mm) and stones ($\phi \geq 60$ mm). Soil samples were previously air-dried and sieved to separate and weigh the coarse and fine-earth fractions. The sieving and sedimentation method (ISO 11277:1998) was used for determining the particle size distribution of the fine-earth fraction.

The thematic maps of soil hydraulic conductivity (K; Fig. 3F), the stone, gravel and sand fraction of the soil (Fig. 3G) and the clay fraction (Fig. 3H) were prepared from the corresponding soil datasets using the Geographic Information System ArcGIS 10.3 for Desktop (ESRI, Redlands, CA, USA; ESRI, 2015) and the ETRS89 UTM Zone 30 N coordinate reference system. To prepare each thematic map, the average value of the two replicated measurements was used for each parameter at each soil sampling point ($n = 259$). The stone, gravel and sand fraction was expressed as a mass percentage of the dry soil. The clay fraction was expressed as a mass percentage of the fine-earth fraction. The raster maps were generated using Inverse Distance Weight (IDW) interpolation in the Spatial Analyst toolbox of ArcGIS and a resolution of 25 m. These thematic maps were used as base maps for preparing three different versions of the S map (Fig. 1): using the parameter S_HC (risk associated with soil hydraulic conductivity; Model 2), using the parameter S_St+G+S (risk associated with the stone, gravel and sand fraction of the soil; Model 3) and using the parameter S_C (risk associated with the clay fraction; Model 4).

2.3. Groundwater nitrate concentration and depth to the water table

The raster maps of nitrate concentration in groundwater (Fig. 2) and depth to the water table (Fig. 3B) were generated using the Spline with Barriers interpolation tool in the Spatial Analyst toolbox of ArcGIS. They were respectively prepared from the mean nitrate concentrations and the mean depths to the water table in 39 sampling points on the Oja aquifer and five on the Tirón aquifer during 2017 (extracted from Arauzo et al., 2022). During the period 2005–2017 no significant decrease was observed in the nitrate pollution of either aquifer (Arauzo et al., 2022).

2.4. Extraction of experimental catchment areas for testing of the vulnerability models

Six experimental catchment areas (Fig. 4) were used to analyse the efficacy of the models for assessing groundwater vulnerability to nitrate pollution and delineating NVZs. Four of these catchments corresponded to the territories that drain into the different polluted zones of the Oja and Tirón aquifers (Fig. 2; Arauzo et al., 2022). The catchments were extracted from a digital elevation model (DEM) of 25 m resolution using the Hydrology toolset in the Spatial Analyst toolbox of ArcGIS. The lowest elevation

Table 1
Characteristics of the Oja and Tirón alluvial aquifers.

Parameter	Oja Alluvial Aquifer	Tirón Alluvial Aquifer
Hydrogeological Domain	Ebro Depression (River Ebro basin, north of Spain)	Ebro Depression (River Ebro basin, north of Spain)
Associated rivers	Rivers Oja and Tirón; Zamaca and Valpierre streams	River Tirón
Aquifer use	Irrigation; human consumption	Irrigation; human consumption
Extent	Floodplains, alluvial fans, first terrace and lower terraces hydraulically connected to the main aquifer	Floodplain, alluvial fans and first terrace
Lithology	Coarse gravels, polygenic gravels and sands with a variable content of silt	Coarse gravels and sands with a variable content of silt
Geology	Quaternary alluvial deposits	Quaternary alluvial deposits
Underlying geology	Conglomerates, sandstones and Miocene shales	Marls and Miocene gypsums
Degree of confinement	Unconfined	Unconfined
Regional Administration	La Rioja	Castilla y León and La Rioja
Total area (km ²)	144	29
Depth to the water table (m)	0–10	0–4
Average thickness (m) ^a	12 (saturated thickness: 7.6)	Not assessed
Resources (hm ³ year ⁻¹) ^a	48–57	Not assessed
Total reserves (hm ³) ^a	170	Not assessed

^a Source: Arauzo et al. (2011).

point of each polluted zone was used as pour point for the watershed calculation (the pour point is the cell of highest flow accumulation). Two other experimental catchment areas were extracted corresponding to territories that drain into non-polluted zones of the upper sections of the aquifers, using the same methodology (Figs. 2 and 4). The surface drainage network and the groundwater flow direction (Fig. 4) were used for catchment delineations. The surface drainage network was generated from a DEM of 25 m resolution using the Hydrology toolset in the Spatial Analyst toolbox. The map of water table elevation was prepared from shapefiles of points of the water table elevation using the Spline with Barriers interpolation tool in the Spatial Analyst toolbox. The shapefiles of points of the water table elevation were previously generated by subtracting the depth to the water table (see Section 2.3) from the corresponding ground surface elevation from a DEM of 25 m resolution.

2.5. Models to assess groundwater vulnerability to nitrate pollution and delineate NVZs

The thematic maps developed for the six models under study were prepared with the Geographic Information System ArcGIS 10.3 for Desktop (ESRI, Redlands, CA, USA; ESRI, 2015) using the ETRS89 UTM Zone 30 N coordinate reference system. The raster layers were generated at a spatial resolution of 25 m.

2.5.1. Model 1: original LU–IV procedure

The original LU–IV procedure (Arauzo, 2107; Arauzo et al., 2019, 2020; Fig. 1) is a two-step GIS-based method that combines a map of intrinsic vulnerability (IV map) with a map of the risk of N-loss associated with land use (LU map). The procedure assigns ratings on a scale from 1 to 10

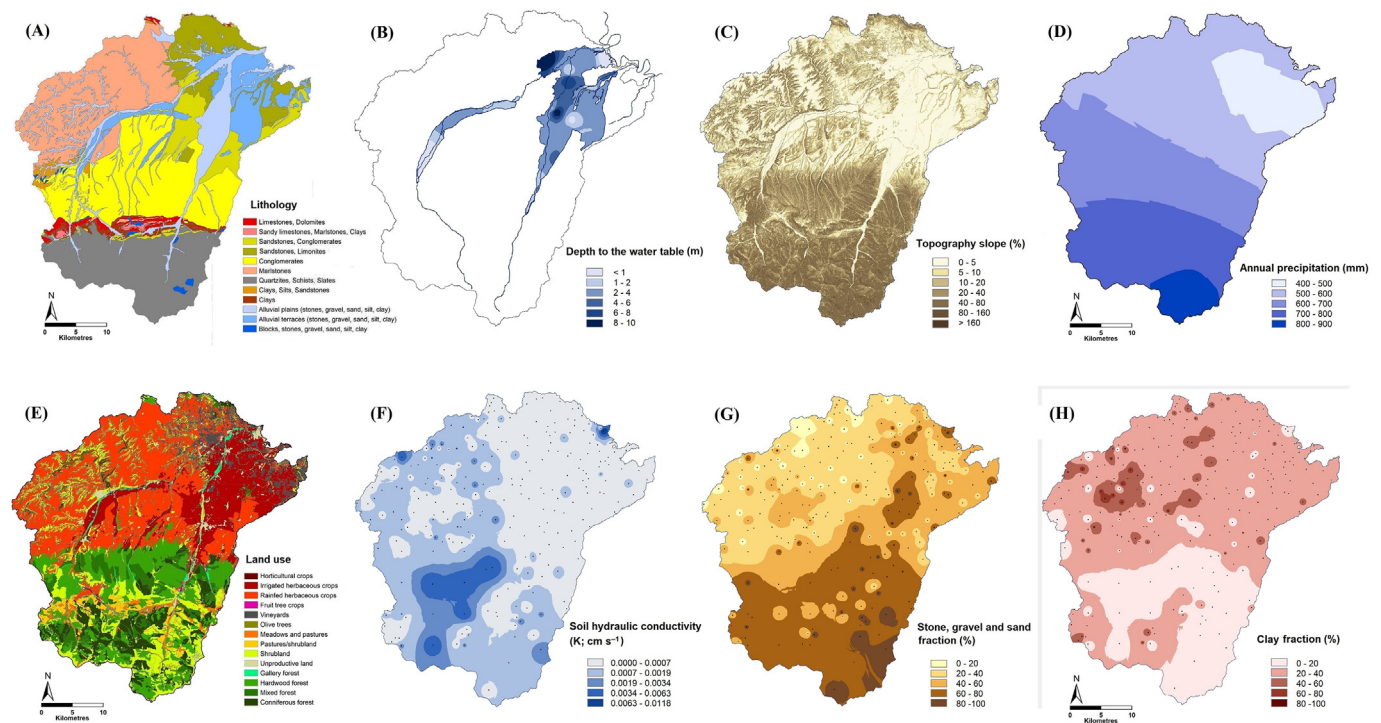


Fig. 3. Thematic maps used in the LU–IV and LU–IV' procedures: (A) lithology, (B) depth to the water table, (C) topography slope, (D) annual precipitation, (E) land use, (F) soil hydraulic conductivity, (G) stone, gravel and sand fraction of the soil, and (H) clay fraction of the fine earth. Locations of the soil sampling points are shown in F, G and H.

Table 2

Ratings for parameters L, D, T, P and LU, which make up the LU–IV procedure (extracted from Tables 3 and 4 in Arauzo et al., 2019).

Parameter	Range	Rating
L: Risk associated with the <u>L</u> ithology of the vadose zone ^a	Karst limestones, calcretes; gravels.	10
	Chalky limestones, calcarenites.	9
	Alluvial and fluvio–glacial sands; recent volcanic lavas.	7–8
	Aeolian sands; volcanic tuffs; fractured igneous and metamorphic formations; older volcanic formations; sandstones, conglomerates; peat.	5–6
	Alluvial silts, loess, glacial till, loam; mudstones; shales.	3–4
D: Risk associated with the <u>D</u> epth to the water table (m) ^b	Clays; residual soils; unfractured igneous and metamorphic formations; other aquifers.	1–2
	0–1 (and all depths for karst limestones, calcretes, gravels, chalky limestones, calcarenites and recent volcanic lavas).	10
	1–3	9
	3–5	8
	5–10	7
	10–13	6
	13–20	5
	20–33	4
	33–50	3
	>50	2
	No underlying aquifer.	1
T: Risk associated with the <u>T</u> opography slope (%) ^c	0–2	10
	2–3	9
	3–4	8
	4–5	7
	5–6	6
	6–9	5
	9–12	4
	12–15	3
	15–18	2
	>18	1
P: Risk associated with <u>P</u> recipitation and irrigation (mm yr ⁻¹ ; in irrigated areas P rating was raised to high risk)	>900	10
	900–800	9
	800–700	8
	700–600	7
	600–500	6 (7) ^d
	500–400	5 (7) ^d
	400–300	4 (7) ^d
	300–200	3 (7) ^d
	200–100	2 (7) ^d
	100–0	1 (7) ^d
LU: N-loss risk associated with <u>L</u> and <u>U</u> se ^e	Horticultural crops (vegetables, root crops and flower crops); citrus crops; irrigated herbaceous forage crops.	10
	Rainfed herbaceous forage crops.	9
	Fruit tree crops.	8
	Irrigated cereals; vineyards; almond trees.	7
	Fish farms; livestock farms; urban areas.	8–5 (7)
	Rainfed cereals; irrigated dried pulses; Irrigated meadows.	6
	Rainfed dried pulses; meadows and pastures; other trees.	5
	Olive trees; irrigated industrial crops.	4
	Rainfed industrial crops.	3
	Shrubland.	5–1 (3)
	Unproductive land.	5–1 (2)
	Forests and natural areas.	1

^a Based on the lithological character and degree of consolidation of vadose zone (Foster et al., 2002) and the hydraulic conductivity and permeability of the media (Bear, 1972).

^b Adapted from Foster et al. (2002).

^c Adapted from Aller et al. (1987).

^d In the irrigated areas (with an additional risk associated with irrigation returns), cell values ranging from 1 to 6 associated with precipitation (negligible to moderate risk) were raised to rating 7 (high risk associated with irrigation) (Arauzo et al., 2020).

^e LU ratings were based on the N-surpluses extracted from the annual reports on N-balances in crops of the Spanish region of La Rioja during 2015 and 2016 (MAPAMA, 2017, 2018; adapted from Arauzo et al., 2019).

for all the parameters (Table 2) and the IV and LU–IV maps, grouped into five risk categories: negligible: 1–2; low: 3–4; medium or moderate: 5–6; high: 7–8; extreme: 9–10.

In step 1, the procedure generates the IV map (map of intrinsic groundwater vulnerability) from the four environmental parameters that comprise the IV index (Fig. 1):

$$IV = \frac{L + D + T + P}{4} \quad (1)$$

where L is the rating of the risk associated with the lithology of the vadose zone, D is the rating of the risk associated with the depth of the water table, T is the rating of the risk associated with the topography slope, and P is the rating of the risk associated with precipitation and irrigation (Table 2).

The IV map was generated from the raster maps L, D, T and P (Fig. 2), using the Raster Calculator in the Spatial Analyst Toolbox of ArcGIS to run Eq. (1).

The L map was prepared from the lithological map of Spain (IGME, 2015; Fig. 3A) by assigning the corresponding L rating to each lithological type (Table 2).

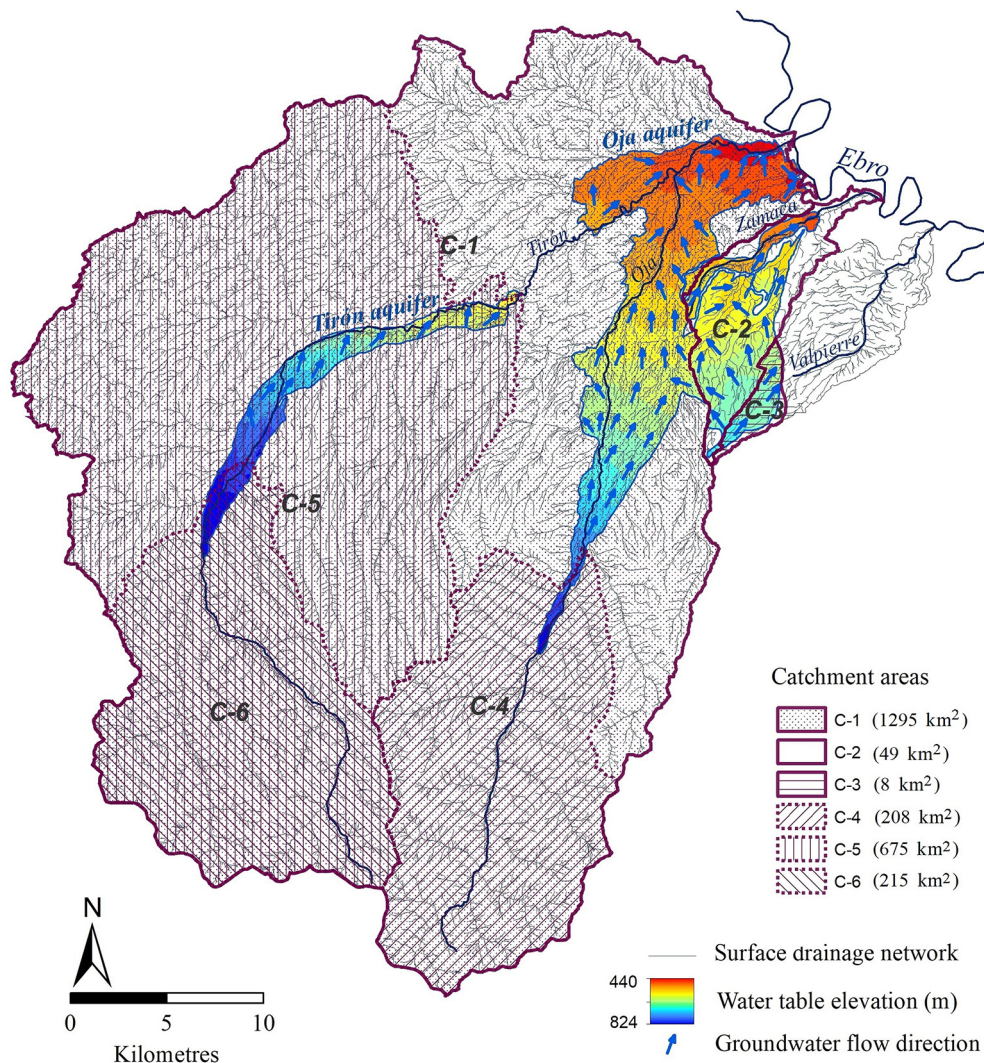


Fig. 4. Surface drainage network and map of water table elevation. Groundwater flow direction is indicated with blue arrows. The catchment areas C-1 to C-6 (extracted to compare the models of groundwater vulnerability to nitrate pollution) are represented with different textures.

The D map was prepared from the depth to the water table map (Fig. 3B) by assigning the corresponding D rating to each depth range (Table 2).

The T map was prepared from the topography slope map (Fig. 3C), which, in turn, was generated from a DEM of 25 m resolution using the Slope tool in the Spatial Analyst Toolbox. T ratings were assigned according to Table 2.

The P map was prepared from the maps of precipitation and irrigation. The map of precipitation (Fig. 3D) was generated from a shapefile of points with the mean annual precipitation during 20 years (22 points of the network of the Spanish Meteorological Agency; Botey et al., 2013) using the IDW interpolation tool in the Spatial Analyst toolbox. To generate the map of the risk associated with precipitation, the P ratings in Table 2 were assigned. The map of the irrigated areas was extracted from the Crops and Land Use map of Spain (MARM, 2009). It was then combined with the map of the risk associated with precipitation using the Logical Math tools in the Spatial Analyst Toolbox so that, in the irrigated areas (with an additional risk associated with irrigation returns), cell values ranging from 1 to 6 associated with precipitation (negligible to moderate risk) were raised to rating 7 (high risk associated with irrigation; Table 2). Only those areas under sprinkler and flood irrigation were considered at risk (Arauzo et al., 2020).

In step 2, the procedure generates the LU-IV map (map of the specific groundwater vulnerability to nitrate pollution) by combining the IV map

(step 1) and the LU map using the Over tool from the Logical Math toolset in the Spatial Analyst Toolbox (Fig. 1). For this, the original raster cell values of the IV map were first reclassified into values 1 and 0. The value 1 represents non-vulnerable areas (cell values ranging from 1 to 4: negligible to low vulnerability), while the value 0 represents vulnerable areas (cell values ranging from 5 to 10: moderate to extreme vulnerability). The resulting raster (IV 1–0 map) was then used as the first entry in the Over tool, while the raster of the N-loss risk associated with land use (LU map) was used as the second entry. When the Over operation is performed, for cell values in the first input that are equal to 1 the output value will be that of the first input (representing areas in which land use restrictions do not have to be applied). But where the cell values in the first input correspond to 0, the output will be that of the second input raster (original ratings of the LU map).

The LU map was previously generated to complete the second entry of the Over tool. This was prepared on the basis of the Crops and Land Use map of Spain (MARM, 2009; Fig. 3E) by assigning the corresponding LU rating to each land use type (Table 2). LU ratings (Table 2) were based on the N-surpluses extracted from the annual reports on N-balances in crops of Spain during 2015 and 2016, in accordance with Arauzo et al. (2019) and adapted to the dataset of La Rioja region (MAPAMA, 2017, 2018). When adapting LU ratings, some ratings varied slightly from those in Arauzo et al. (2019): irrigated cereals from 8 to 7, rainfed cereals from 7 to 6, vineyards from 6 to 7, and fruit tree crops from 9 to 8 (Table 2).

Table 3
Ratings for parameters S of the index IV' (Models 2, 3 and 4).

Parameter S	Range	Rating
Model 2: Parameter S _{HC} ; risk associated with soil Hydraulic Conductivity (K; cm s ⁻¹) ^a	>0.007	10 ^e
	0.007–0.005	9 ^e
	0.005–0.003	8 ^e
	0.003–0.002	7 ^e
	0.002–0.0009	6 ^e
	0.0009–0.0004	5 ^e
	0.0004–0.0002	4
	0.0002–0.00006	3
	0.00006–0.00004	2
	<0.00004	1
Model 3: Parameter S _{St+G+S} ; risk associated with the Stone, Gravel and Sand fraction (%) ^{b, c}	100–98	10 ^e
	98–80	9 ^e
	80–66	8 ^e
	66–55	7 ^e
	55–46	6 ^e
	46–38	5 ^e
	38–30	4
	30–23	3
	23–14	2
	14–0	1
Model 4: Parameter S _C ; risk associated with the Clay fraction (%) ^{c, d}	0–17	10 ^e
	17–27	9 ^e
	27–31	8 ^e
	31–33	7 ^e
	33–35	6 ^e
	35–39	5 ^e
	39–49	4
	49–68	3
	68–98	2
	98–100	1

^a Based on FAO and USDA hydraulic conductivity classes (FAO, 2021; USDA, 2021).

^b Expressed as a mass percentage of the dry soil.

^c Based on drainage data from a network of lysimeters in the study area (Arauzo and Valladolid, 2013).

^d Expressed as a mass percentage of the fine-earth fraction.

^e Cell values ranging from 5 to 10 (moderate to extreme risk) were reduced to 4 (low risk) in soils with petrocalcic or clay horizons (Gobierno de La Rioja, 2006b) and a topography slope below 5 % (petrocalcic and clay horizons limit vertical drainage and low slopes limit subsurface runoff in the vadose zone).

The map of groundwater vulnerability to nitrate pollution (LU–IV map; Fig. 1), which combines information from the physical environment and land use, will serve as a base map to delineate the NVZs. More details on this methodology can be consulted in Arauzo (2017) and Arauzo et al. (2019, 2020).

2.5.2. Model 2 (NEW): LU–IV' procedure using the parameter S_{HC}

The LU–IV' procedure is similar to that of Model 1 except that, in step 1, the IV' index is composed of five parameters instead of four (Fig. 1), as follows:

$$IV' = \frac{L + D + T + P + S}{5} \quad (2)$$

Parameters L, D, T and P are the same as in Model 1. The new parameter S represents the risk associated with soil permeability. Three easily estimable parameters related to soil permeability were selected to be tested as parameter S: the risk associated with soil hydraulic conductivity (parameter S_{HC}; Model 2), the risk associated with the stone, gravel and sand fraction of the soil (parameter S_{St+G+S}; Model 4), and the risk associated with the clay fraction (parameter S_C Model 4). The objective was to know which would be the most effective for assessing groundwater vulnerability.

In Model 2, the S map (Fig. 1) was prepared from the map of soil hydraulic conductivity (K; Fig. 3F) by assigning the corresponding S rating to each range of hydraulic conductivity (Table 3). S_{HC} ratings (Table 3) were based on FAO and USDA hydraulic conductivity classes (FAO, 2021; USDA, 2021).

Step 2 of the LU–IV' procedure was the same as for Model 1, but using the IV' index with the parameter S_{HC}.

S maps of Models 2 to 4 were adapted in those areas with petrocalcic or clay horizons (that limit vertical drainage) and low slopes (that limit subsurface runoff in the vadose zone). For this, cell values with ratings from 5 to 10 (moderate to extreme risk) were reduced to 4 (low risk) in soils with petrocalcic or clay horizons (Gobierno de La Rioja, 2006b) and a topography slope below 5 % (Fig. 3C).

2.5.3. Model 3 (NEW): LU–IV procedure using the parameter S_{St+G+S}

Model 3 is similar to Model 2, except that the S map (Fig. 1) was prepared from the map of the stone, gravel and sand fraction (S_{St+G+S}; Fig. 3G) by assigning the corresponding S ratings to the different ranges (Table 3). S_{St+G+S} ratings were established from drainage data from a network of lysimeters in the study area (Arauzo and Valladolid, 2013).

Step 2 of the LU–IV' procedure was the same as for Model 1, but using the IV' index with the parameter S_{St+G+S}.

2.5.4. Model 4 (NEW): LU–IV procedure using the parameter S_C

Model 4 is similar to Model 2, except that the S map (Fig. 1) was prepared from the map of the clay fraction (S_C; Fig. 3H) by assigning the corresponding S ratings to the different ranges (Table 3). S_C ratings were established from drainage data from a network of lysimeters in the study area (Arauzo and Valladolid, 2013).

Step 2 of the LU–IV' procedure was the same as for Model 1, but using the IV' index with the parameter S_C.

2.5.5. Model 5 (NEW): LU–DRASTIC–COP procedure

Model 5 uses the DRASTIC index (Aller et al., 1987) and the COP index (Vías et al., 2006) to assess the intrinsic vulnerability. The Geological and Mining Institute of Spain (IGME) mapped the intrinsic vulnerability of Spanish aquifers on a national scale using these methods. The maps of intrinsic vulnerability of detrital and mixed aquifers, based on DRASTIC (IGME, 2009a), and of carbonate aquifers, based on COP (IGME, 2009b), were used as base maps to generate the DRASTIC–COP map of intrinsic vulnerability of Model 5 (Fig. 5).

The DRASTIC index uses seven parameters (depth to the water table, aquifer recharge, aquifer media, soil media, topography, impact of vadose zone and hydraulic conductivity) in an additive formulation, which are weighted according to their relative importance to the pollution potential (Aller et al., 1987). The COP method uses three main parameters (concentration of flow, overlaying layers above the water table and precipitation over the aquifer) in a multiplicative formulation (Vías et al., 2006). The original ratings of DRASTIC and COP were transformed to a scale of 1 to 10 to make them comparable to those of the previous models.

As in step 2 of the LU–IV procedure, the DRASTIC–COP map of intrinsic vulnerability was reclassified into values 1 and 0 to generate the DRASTIC–COP 1–0 map, which was combined with the LU map using the Over tool to generate the LU–DRASTIC–COP map of specific groundwater vulnerability to nitrate pollution.

2.5.6. Model 6: officially designated NVZ

The only zone within the study area designated as a NVZ (Gobierno de La Rioja, 2006a) covers the most polluted sections of the Oja aquifer (Fig. 2 and Table 2), with nitrate concentration in groundwater probably being the criterion for the designation. However, no designations were made on the Tirón aquifer following that criterion. Although the vulnerability model used for designations in the study area was unknown to us, it was considered necessary to compare the officially designated NVZs with those obtained from the previous models to find the most effective model. For this reason, despite not knowing the characteristics of the model, the officially designated NVZ was defined as Model 6.

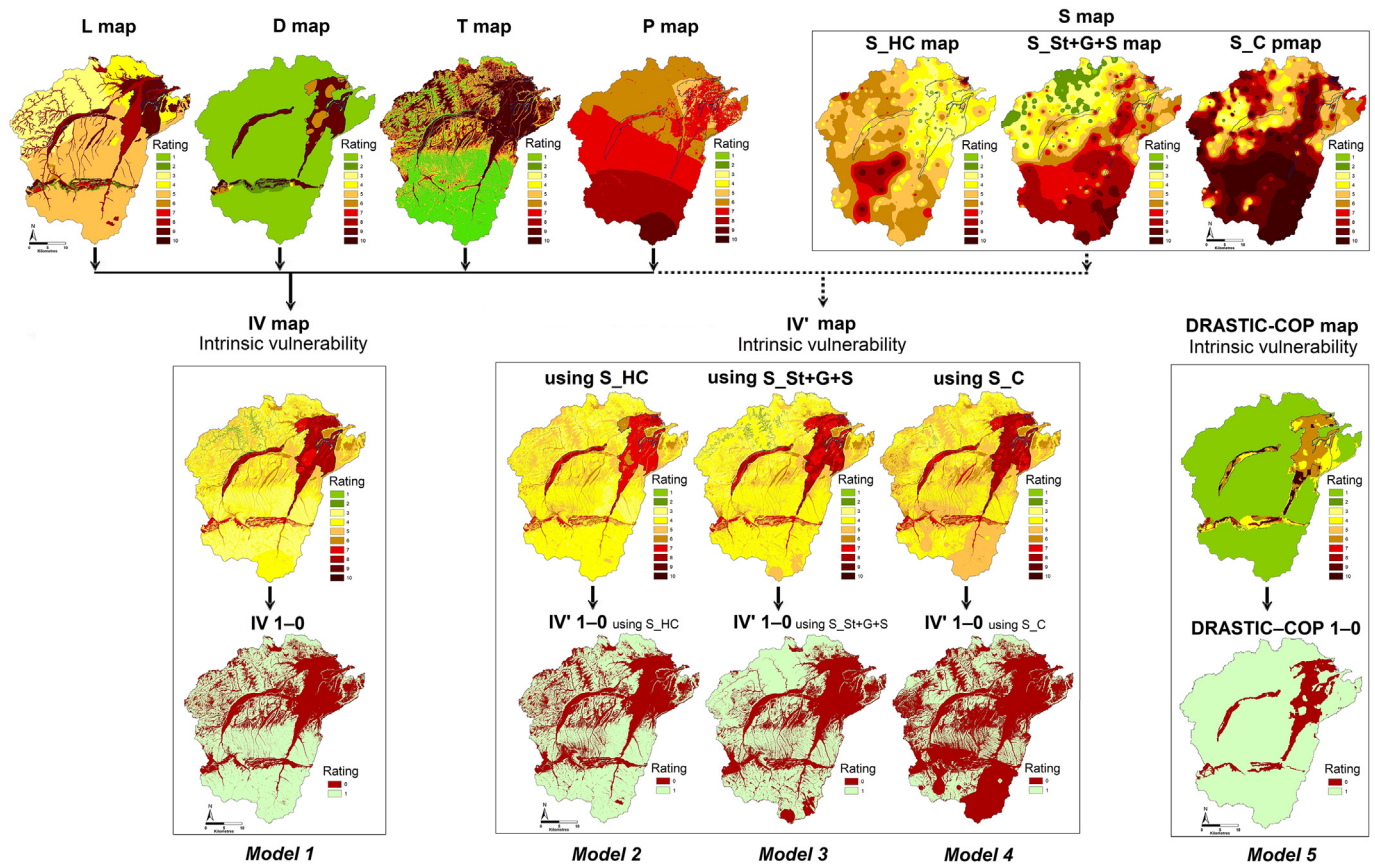


Fig. 5. Maps of intrinsic groundwater vulnerability based on the IV index (four parameters: L, D, T and P; Fig. 1) and the IV' index (five parameters: L, D, T, P and S; Fig. 1). Three different parameters related to the risks associated with soil permeability (parameter S) were tested: parameter S_{HC} (risk associated with soil hydraulic conductivity), parameter S_{St + G + S} (risk associated with the stone, gravel and sand soil fraction) and parameter S_C (risk associated with the clay fraction). The maps of the risks associated with the environmental parameters that make up the indexes are shown at the top of the figure.

2.6. Statistical analysis

Single-parameter sensitivity analyses of the IV and IV' indices were performed to look for possible differences between the theoretical weights assigned to the parameters of each index (equal for all parameters) and their effective counterparts. The following equation was used:

$$W = \left(\frac{Pr * Pw}{V} \right) * 100 \quad (3)$$

where W is the effective weight of each parameter, Pr and Pw are the rating and theoretical weight assigned to each parameter, respectively, and V is the value of the vulnerability index (Babiker et al., 2005). For the IV index (four parameters: L, D, T and P; Eq. (1)), the value of Pw is equal to ¼ for every parameter. For the IV' index (five parameters: L, D, T, P and S; Eq. (2)), the value of Pw is equal to ⅕. The IV' index from Model 2 (where parameter S represents the risk associated with soil hydraulic conductivity) was used to perform the analysis. The single-parameter sensitivity analyses were conducted using the Raster Calculator in the Spatial Analyst toolbox of ArcGIS, grid by grid, from maps L, D, T, P, S, IV and IV' (Fig. 1).

Pearson correlations between pairs of thematic rasters were conducted using Band Collection Statistics in the Spatial Analyst toolbox. Correlations between the raster maps L, D, T and P and the raster maps S_{HC}, S_{St + G + S} and S_C were used to explore relationships between the parameters that make up the original IV index and the new parameters included in the IV' index. A Pearson correlation matrix of the raster maps of NVZs resultant from the six models under study was also used to analyse the relationships

between the models. The number of pairs in the correlations corresponded to the number of pixels in the rasters (2,235,134).

The assessment of the vulnerability of groundwater to nitrate pollution under a 'source-pathway-receptor' approach (Machiwal et al., 2018) involves considering that nitrate can be displaced long distances from the highest to the lowest areas of the basins (Zahid et al., 2015), not only in the saturated zone of the aquifers but also in the vadose zone of their catchment areas. If the NVZs are well delineated, a direct relationship can be expected between the area defined as NVZ in the catchment area of an aquifer and the area polluted by nitrate of the aquifer (Arauzo, 2017; Arauzo et al., 2019). Bearing this in mind, to compare the robustness of the six models under study, the Spearman correlations (Rho; IBM SPSS Statistics 27.0; IBM Corp. Released, 2020) were determined between the areas of NVZs (extracted for each of the models) vs the alluvial areas polluted by nitrate, using datasets extracted from the six experimental catchment areas. The datasets were obtained, catchment by catchment, from catchments C-1 to C-6 (Fig. 4; n = 6) using the Spatial Analyst toolbox. The correlations were performed on the percent coverages of NVZs and alluvial areas polluted by nitrate in each catchment. The percent coverage of NVZs was expressed as the relative area at high to extreme risk (ratings 7–10) over the catchment area. The percent coverage of alluvial areas polluted by nitrate was expressed as the relative area above 50 mg L⁻¹ of nitrate over the total alluvial area and the catchment area. The Shapiro-Wilk normality test was used to check the assumption of normality (IBM SPSS Statistics 27.0), which was not satisfied for any of the datasets. The efficacy of the intrinsic vulnerability indices (step 1 in Models 1 to 5) to estimate NVZs was also explored using Spearman correlations in the same way and under the same conditions as stated above. In those cases, the percent coverage of

vulnerable areas was also expressed as the relative area at high to extreme risk over the catchment area.

3. Results and discussion

3.1. Nitrate polluted zones and their catchment areas

Nitrate distribution in groundwater is a consequence of nitrate high solubility and mobility through the vadose and saturated zones (Arauzo et al., 2022). No significant decrease in nitrate pollution has been observed in the Oja and Tirón aquifers since the 2006 NVZ designation (Arauzo et al., 2022; Fig. 2). The high groundwater flow velocity at the upper reaches of both aquifers favours advective nitrate transport toward the lower reaches and with low water flow, where it tends to accumulate in stagnation zones (Arauzo et al., 2011). A total of five zones with persistent pollution by nitrate were identified (Fig. 2): (zone 1) lower reaches of the Oja aquifer, (zone 2) branch of the Zamaca stream and upper section of the Valpierre stream (southeastern area of the Oja aquifer), (zone 3) right bank of the river Oja, (zone 4) left bank of the river Oja and (zone 5) mid-lower section of the Tirón aquifer. Arauzo and Martínez-Bastida (2015), Arauzo et al. (2011, 2022), Orellana-Macías et al. (2020), Richard et al. (2018) and Worrall et al. (2009) noted that when NVZs are poorly delineated, expectations of significantly reducing nitrate pollution in groundwater bodies are not met. That could be the case in the territory under study, which points to the need to review its NVZs.

Since the main objective of this research was to compare the efficacy of different models for assessing the vulnerability of groundwater to nitrate pollution and delineating NVZs in the context of the hydrological catchment, datasets were extracted from six experimental catchment areas with different hydrology, lithology, topography, precipitation, catchment size, soils, land use and degree of nitrate pollution (Fig. 4). Four of the catchments drain into zones with persistent nitrate pollution (Fig. 2): C-1 (affecting zones 1, 3, 4 and 5, in the main body of the Oja aquifer and the Tirón aquifer), C-2 (affecting zone 2, in the branch of the Zamaca stream), C-3 (affecting zone 2, in the upper section of the Valpierre stream) and C-5 (affecting zone 5, in the Tirón aquifer). The two other experimental catchments drain into non-polluted zones of the aquifers: C-4 (that drains into the upper reaches of the Oja aquifer) and C-6 (that drains into the upper reaches of the Tirón aquifer). Catchments C-1 and C-5 are the largest in size; with mountains at the headwaters that are associated with higher precipitations. They show <45 % of the alluvial areas polluted by nitrate, which constitutes <3 % of the catchment area. More than 50 % of their surface is covered by forests and natural areas at the headwaters, while rainfed herbaceous crops are dominant in the lower zones (Table 4). Catchments C-2 and C-3 are the smallest in size and are characterised by over 80 % polluted alluvial areas, covering 66 % of the catchment area. They are flat territories, with precipitation lower than 600 mm and >69 % of the surface covered by irrigated herbaceous crops (Table 4). Catchments C-4 and C-6 correspond to the headwater areas. They are free of nitrate pollution, have high slopes and precipitation and a forest cover of 92 % (Table 4). In the following sections, datasets from all these experimental catchments, extracted catchment by catchment, will be used to establish statistical comparisons between the coverages of NVZs estimated from each of the six models under study and those of alluvial zones polluted by nitrates.

3.2. Intrinsic vulnerability

This research intends to refute the idea that aquifer recharge is produced only by vertical infiltration, on which most methods for mapping groundwater vulnerability are based. Recharge can also come from places far away from the aquifer (Arauzo, 2017; Arauzo and Martínez-Bastida, 2015; Zahid et al., 2015), so the entire surface of the catchment area that drains into the aquifer should be evaluated, or better, the whole surface of the territory. That is precisely one of the differential characteristics of the LU-IV procedure and begins from step 1 of the procedure. Step 1 of Models 1 to 4 assessed the intrinsic vulnerability throughout the entire

territory (IV map and IV' maps using S_HC, S_St + G + S and S_C; Fig. 5). Model 5, however, only evaluated the land surface above groundwater bodies (DRASTIC-COP map; Fig. 5).

For Models 2 to 4, it was hypothesized that the vulnerability assessment would improve by including a parameter representing the risk associated with soil permeability (parameter S) in the procedure. Although Aller et al. (1987), Arauzo et al. (2022) and Witkowski et al. (2007) highlight the role of soil permeability in infiltration and its impact on groundwater vulnerability, the scarcity of georeferenced data on soil permeability could pose a limitation to correctly feeding these types of models, affecting their robustness. To test the hypothesis, three different versions of parameter S, based on the soil hydraulic conductivity (parameter S_HC), the fraction of stone, gravel and sand (parameter S_St + G + S) and the clay fraction (parameter S_C), were used. Variability of the three parameters in the study area was high, ranging from 0 to 0.01 cm s⁻¹, 7 % to 95 % and 0 % to 76 %, respectively (Fig. 3F, G, H).

The IV and IV' maps (Models 1 to 4) showed a high to extreme risk for the alluvial and carbonate deposits. In addition, they showed a medium risk for territories without underlying groundwater bodies (Fig. 5), from which nitrate could reach groundwater via the surface drainage network or sub-surface runoff. The DRASTIC-COP map (Model 5) showed a medium to extreme risk for the alluvial and carbonate deposits (with minor areas of low risk), but did not analyse the areas without underlying groundwater (Fig. 5).

Regarding the relationship between parameters that make up the original IV index (L, D, T and P) and those added to the IV' indexes (S_HC, S_St + G + S and S_C), statistically significant correlations were found between the two sets of parameters (Table 5). Negative correlations of parameters S_HC, S_St + G + S and S_C vs parameter T and positive correlations vs parameter P stand out as the most significant. The IV and IV' maps show that the inclusion of the different versions of the parameter representing the risk associated with soil permeability in Models 2 to 4 refined results compared to Model 1, but without any significant changes (Fig. 5). Correlations between parameters (Table 5) explain this fact.

Maps of intrinsic vulnerability in Fig. 5 were reclassified into values of 1 and 0 to identify the areas at medium to extreme risk (a conservative criterion to ensure including all possible intrinsically vulnerable areas for step 2 of the procedure; Arauzo et al., 2020).

Reclassifications tended to homogenise the results of the five models in the alluvial and carbonate areas but not in the rest of the territory (Fig. 5). According to maps IV 1-0, IV' 1-0 using S_HC, IV' 1-0 using S_St + G + S and IV' 1-0 using S_C, and DRASTIC-COP 1-0 (Fig. 5), Model 1 showed a surface area at medium to extreme risk of 514 km² (37 % of the study area), Model 2 of 530 km² (38 %), Model 3 of 531 km² (38 %), Model 4 of 881 km² (63 %) and Model 5 of 182 km² (13 %). Surfaces identified as intrinsically vulnerable were similar for Models 1 to 3, although Model 3 presented a somewhat different distribution. Model 4 showed a vulnerable area almost a third higher than the previous ones, while Model 5 only identified their third part (Fig. 5). Discrepancies between models at the end of step 1 could lead (Fig. 5), in turn, to amplifying the dispersion of their results at step 2 of the procedure. This issue will be addressed in the following sections.

Unlike the DRASTIC index, the IV and IV' indexes assign the same theoretical weight to their parameters to minimize the impact of the subjective component linked to the pre-assignment of different weights (Javadi et al., 2011). The IV index (made up of four parameters) assigns a weight of ¼ to each parameter, while the IV' index (made up of five parameters) assigns a weight of ⅕. Single-parameter sensitivity analyses to compare the theoretical weight assigned to parameters of the IV index (Model 1) and the IV' index (Model 2) vs their effective weight (Table 6) showed that the theoretical and effective weights were similar for most of the parameters in both models, except for parameters P and D whose mean effective weights were, respectively, higher and lower than their theoretical weights. The high variability observed of the effective weights of the parameters throughout the study area (Table 6) reinforces the idea suggested by Arauzo (2017) and Babiker et al. (2005) that the individual characteristics

Table 4
Characteristics of the six experimental catchment areas.

Parameter	Catchment C-1	Catchment C-2	Catchment C-3	Catchment C-4	Catchment C-5	Catchment C-6
Receptor aquifer	Tirón aquifer and main body of Oja aquifer (polluted)	Zamaca branch of Oja Aquifer (polluted)	Valpierre section of Oja aquifer (polluted)	Upper reaches of Oja aquifer (unpolluted)	Tirón aquifer (polluted)	Upper reaches of Tirón aquifer (unpolluted)
Associated rivers	Rivers Oja and Tirón	Zamaca stream	Upper reaches of Valpierre stream	Upper reaches of River Oja	Upper-middle reaches of River Tirón	Upper reaches of River Tirón
Catchment area (km ² ; CA)	1295	49	8	208	675	205
Alluvial area (km ² ; AA)	132	34	7	2	29	5
Altitude (m; max.–mean–min.)	2270–911–433	699–56–427	695–639–605	2270–1255–704	2039–948–547	2039–1199–730
Designated NVZ (km ²)	56	38	0	0	0	0
Land use ^{a, b}						
Irrigated herbaceous crops, horticultural crops	11 %	69 %	70 %	1 %	6 %	1 %
Rainfed herbaceous crops	32 %	14 %	26 %	0 %	40 %	3 %
Vineyards	3 %	9 %	1 %	0 %	0 %	0 %
Meadows, pastures	2 %	0 %	0 %	4 %	2 %	3 %
Forest, natural areas, shrubland	50 %	5 %	2 %	92 %	51 %	92 %
Unproductive land	2 %	3 %	1 %	2 %	1 %	1 %
Coverage of irrigated land (sprinkling and furrow)	11 %	67 %	30 %	1 %	5 %	1 %
Lithology ^a						
Alluvial deposits	15 %	85 %	84 %	8 %	15 %	9 %
Limestones	2 %	0 %	0 %	4 %	3 %	4 %
Sandstones, conglomerates, slates, schists	48 %	15 %	16 %	85 %	46 %	82 %
Marlstones	34 %	0 %	0 %	0 %	36 %	1 %
Clays	1 %	0 %	0 %	3 %	0 %	4 %
Slope ^a						
0–5 %	34 %	82 %	100 %	5 %	31 %	7 %
5–9 %	13 %	12 %	0 %	3 %	15 %	8 %
> 9 %	53 %	6 %	0 %	92 %	54 %	85 %
Precipitation ^a						
600–900 mm y ⁻¹	58 %	0 %	0 %	100 %	70 %	100 %
400–600 mm y ⁻¹	42 %	100 %	100 %	0 %	30 %	0 %
Soil characteristics ^c						
Dominant soil texture	Clay/ Clay loam/ Loam/ Sandy loam	Clay loam/ Loam	Clay loam/ Loam	Loam/ Sandy loam	Clay/ Silty loam/ Sandy loam	Sandy loam
Fine soil fraction: Sand–Silt–Clay (%)	35 (18)–35 (15)–30 (15)	39 (5)–33 (4)–28 (4)	43 (2)–19 (5)–38 (2)	50 (12)–35 (8)–15 (8)	33 (20)–34 (20)–33 (19)	53 (20)–21 (14)–26 (17)
Coarse soil fraction (%)	27 (25)	25 (15)	45 (1)	51 (25)	26 (25)	47 (26)
Soil hydraulic conductivity (K; cm s ⁻¹)	0.0008 (0.0001)	0.0003 (0.0003)	0.0001 (0.0000)	0.0008 (0.0008)	0.0012 (0.0013)	0.0015 (0.0017)
Nitrate pollution ^d						
Alluvial area polluted by nitrate over the total alluvial area (% AA)	34 %	95 %	80 %	0 %	45 %	0 %
Alluvial area polluted by nitrate over the total catchment area (% CA)	3 %	66 %	66 %	0 %	2 %	0 %

^a Percent coverage over the catchment area (% CA).

^b Extracted from the Crops and Land Use map of Spain (MARM, 2009).

^c Mean value from the soil sampling points; standard deviations in brackets.

^d Percent coverage of the alluvial areas above 50 mg L⁻¹ of nitrate (% AA).

of the unit of analysis (e.g. pixel; catchment; region) can affect the resulting effective weights. These results point to the convenience of not pre-assigning different weights to the input parameters of the vulnerability indexes in order to avoid inaccuracies (Hamza et al., 2015). They also could explain discrepancies between Models 1 to 4 and Model 5 in assessing intrinsic vulnerability.

3.3. Specific vulnerability to nitrate pollution

This investigation analyses and compares the efficacy in NVZ delineation of different models for assessing the vulnerability of groundwater to

nitrate pollution (Fig. 6) that combine maps of intrinsic vulnerability (Models 1 to 5; Fig. 5) with a map of the risk of N-loss associated with land use (LU map; Fig. 6). According to the LU map (Fig. 6), intensive agriculture is widely implanted in the alluvial areas and their surrounding territories, which potentially poses a high to extreme risk of N-leaching. Rainfed agriculture (mainly cereals) is distributed throughout the rest of the middle and lowlands (posing a medium risk of N-loss), while forests and natural areas are limited to the mountain areas (constituting a protecting factor against nitrate pollution) (Arauzo et al., 2022).

Models 1 to 4 showed a surface area with high to extreme vulnerability to nitrate pollution of 204–227 km², Model 5 of 112 km² and Model 6 of 94 km² (in red, Fig. 6; Table 7). The areas at high to extreme vulnerability were considered potentially designatable NVZs. They covered 15–16 % of the territory for Models 1–4, 8.0 % for Model 5 and 6.7 % for Model 6 (NVZ officially designated in 2006).

Results of Models 1 to 4 (original LU–IV procedure and LU–IV' procedures using the parameters S_{HC}, S_{St} + G + S and S_C) were close, not only in terms of the percent coverage of estimated NVZs but also in their spatial distribution. Proof of this was the highly significant correlations between their respective rasters (Table 7), although Model 2 identified a smaller vulnerable area and Model 4 a larger one than Models 1 and 3. The estimated NVZs from Models 1 to 4 covered most of the alluvial areas

Table 5
Pearson correlations between the rasters L, D, T and P and the rasters S_{HC}, S_{St} + G + S and S_C (Fig. 5) to explore relationships between the parameters that make up the original IV index and those added in its new versions (IV' indexes); degrees of freedom: 2,235,132; all the results are significant at $p < 0.00001$.

	L	D	T	P
S _{HC}	−0.22	−0.24	−0.44	0.43
S _{St} + G + S	0.08	−0.06	−0.54	0.69
S _C	0.02	−0.01	−0.39	0.53

Table 6

Effective weights from single-parameter sensitivity analyses (W; Eq. (3)) compared with theoretical weights for the IV index of Model 1 (four parameters: L, D, T and P) and the IV' index of Model 2 (five parameters: L, D, T, P and S).

Intrinsic vulnerability	Parameter	Theoretical weight (Pw; %)	Mean effective weight (W; %)	SD	Minimum effective weight (%)	Maximum effective weight (%)	n
IV index (Model 1)	L	25	27	77	7	66	2,235,134
	D	25	10	66	3	56	2,235,134
	T	25	24	230	3	62	2,235,134
	P	25	39	222	15	87	2,235,134
IV' index (Model 2)	L	20	21	38	5	60	2,235,134
	D	20	8	54	2	50	2,235,134
	T	20	19	167	2	53	2,235,134
	P	20	29	68	14	70	2,235,134
	S	20	22	66	2	53	2,235,134

SD: standard deviation; n: number of values (pixels) used to compute the analysis.

and their surrounding territories, under intensive agriculture, both in the Oja and Tirón aquifers. The initial hypothesis that vulnerability assessment can improve by including a parameter representing the risk associated with soil permeability (parameter S) in step 1 of the LU-IV' procedure seems, therefore, weak. Convergent results of Models 1–4 suggest that the inclusion of that parameter could be unnecessary. On the other hand, Models 1–4 also provided information on zones with medium vulnerability to nitrate pollution (in orange, Fig. 6), which covered a surface area of 199 km² (14 % of the territory) for Models 1 and 2, 144 km² (10 %) for Model 3 and 280 km² (20 %) for Model 4. Arauzo and Valladolid (2013) reported significant N-losses to groundwater from rainfed herbaceous crops

associated with precipitation as a triggering factor in the area. Therefore, zones with medium vulnerability to nitrate pollution could also be controlled for a more effective and quick recovery of groundwater quality.

NVZs estimated from Model 5 (LU-DRASTIC-COP procedure) covered somewhat less alluvial surface area than previous models (in red; Fig. 6). Model 5 does not analyse the territories without underlying groundwater so that, outside the alluvial areas, only small surfaces of other detrital and carbonate deposits were identified as vulnerable. Model 6 shows the officially designated NVZ (Gobierno de La Rioja, 2006a), which covers the most polluted sections of the Oja aquifer, but with no designations in the Tirón aquifer (in red; Fig. 6). It covers the zones of the Oja Alluvial Aquifer

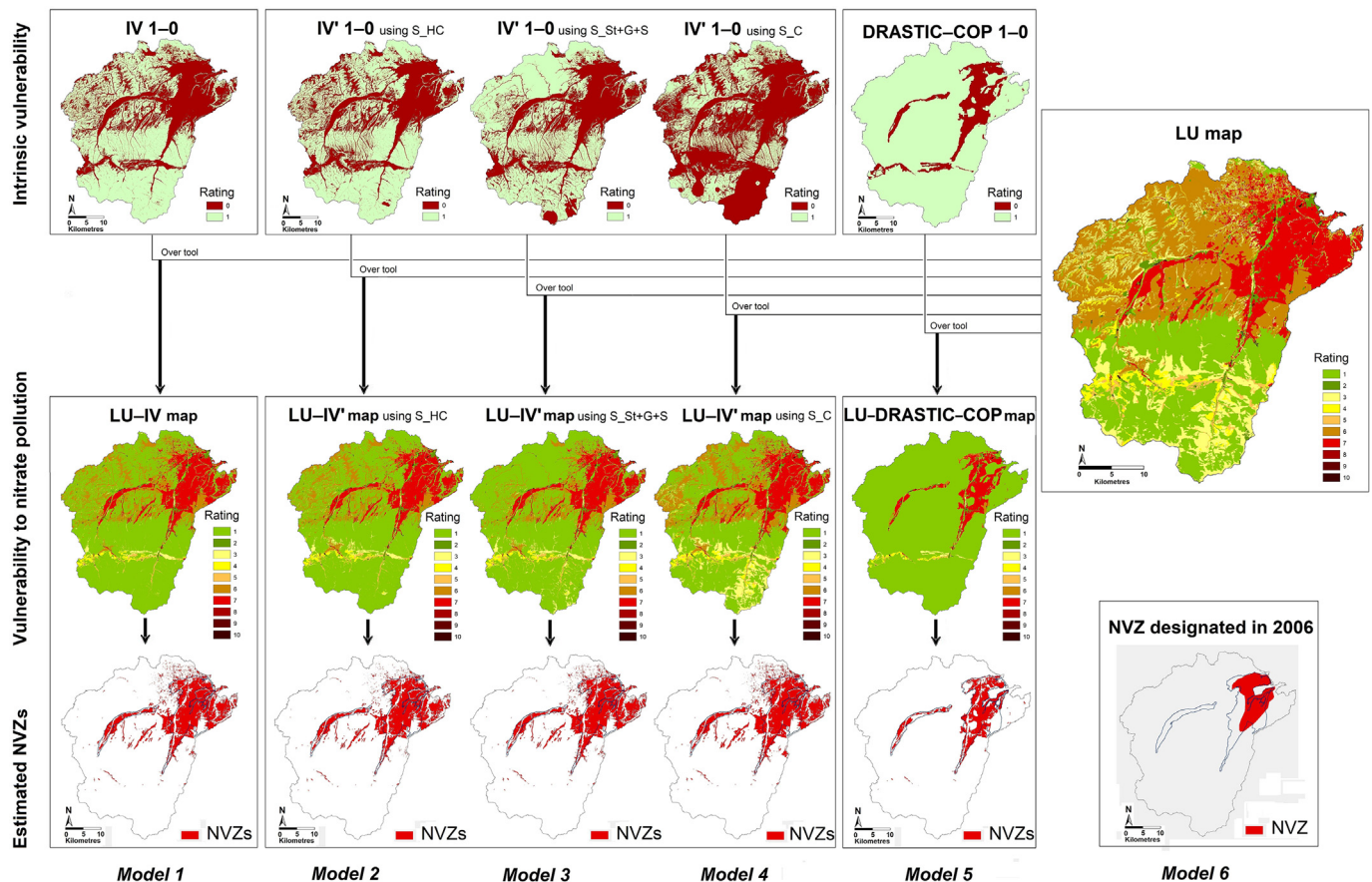


Fig. 6. Maps of specific groundwater vulnerability to nitrate pollution and estimated NVZs based on: Model 1 (LU-IV procedure; Arauzo, 2017), Model 2 (LU-IV' procedure using the parameter S_{HC}), Model 3 (LU-IV' procedure using the parameter S_{St}+G+S), Model 4 (LU-IV' procedure using the parameter S_C) and Model 5 (LU-DRASTIC-COP model). Maps of intrinsic vulnerability 1–0 (moderate to extreme) and LU map (N-loss risk associated with land use) that make up the procedures are shown above. For comparison, the officially designated NVZ (Gobierno de la Rioja, 2006a) is represented as Model 6.

Table 7

Pearson correlation matrix of the rasters of NVZs resultant from the six models (Fig. 6); degrees of freedom: 2,235,132; all the results are significant at $p < 0.00001$. The area of NVZs estimated from each model is indicated in brackets.

	NNZs from Model 1	NNZs from Model (NEW)	NNZs from Model 3 (NEW)	NNZs from Model 4 (NEW)	NNZs from Model 5 (NEW)	NNZs from Model 6
NNZs from Model 1 [216 km ²]	1.00					
NNZs from Model 2 (NEW) [204 km ²]	0.96	1.00				
NNZs from Model 3 (NEW) [215 km ²]	0.98	0.96	1.00			
NNZs from Model 4 (NEW) [227 km ²]	0.97	0.94	0.97	1.00		
NNZs from Model 5 (NEW) [112 km ²]	0.68	0.69	0.68	0.66	1.00	
NNZs from Model 6 [94 km ²]	0.48	0.49	0.48	0.47	0.54	1.00

where nitrate tends to accumulate (Fig. 2) but not its sources of origin. The correlation matrix of the rasters of NVZs estimated from the six models (Table 7) shows that Models 5 and 6, although statistically significant, presented weaker correlations with each other and with Models 1–4.

3.4. Model validations on a catchment by catchment basis

Scientific literature shows that the correlation between nitrate contents in groundwater and levels of vulnerability (from rasters or simply from datasets of groundwater sampling points) has been widely used in validating vulnerability models (Boy-Roura et al., 2013; Kura et al., 2015; Martínez-Bastida et al., 2010). This excessively simplistic approach assumes that nitrate only reaches the aquifer through vertical infiltration from its surface, disregarding long-distance displacement of nitrate from the highest to the lowest areas of aquifers catchment areas (Arauzo, 2017; Arauzo and Martínez-Bastida, 2015; Zahid et al., 2015). It would be, therefore, more realistic to analyse the vulnerability and validate the models in the context of the catchment, which allows considering N-transport by surface runoff, infiltration, subsurface runoff in the vadose zone (in sloping areas) and advective transport and accumulation/dilution within the saturated zone. To compare the robustness of the six models of vulnerability, validations at the catchment scale were conducted using datasets extracted from the experimental catchment areas C–1 to C–6 (Fig. 4). Four of these catchments drain into polluted zones and the two others into non-polluted ones (Table 4), offering together the necessary environmental variability (in size, altitude, lithology, topography, weather conditions, soil and land use) to address model validations. Similar, highly significant correlations were observed between the percent coverages of the NVZs and the percent coverages of the alluvial areas polluted by nitrates for Models 1–4 (original LU–IV procedure and LU–IV' procedures using parameters S_{HC}, S_{St} + G + S and S_C, respectively; Table 8). Model 5 (LU–DRASTIC–COP procedure) and Model 6 (official NVZ) did not show any significant results (Table 8). In light of these results, Models 1–4 have proven to be the best predictors of nitrate pollution in alluvial areas, showing similar fits to the validation data, making all of them good models for NVZ delineation. As stated in the previous section, Models 1–4 were close in their NVZ estimations, which covered most of the alluvial areas of the Oja and Tirón aquifers and surrounding territories under intensive agriculture. These results

support the idea that including a parameter representing the risk associated with soil permeability in the LU–IV' procedure (Models 2–4) is not essential since equivalent results were obtained from the LU–IV procedure (Model 1).

On the other hand, the efficacy of the intrinsic vulnerability indices (Fig. 5; Table 9) as estimators of NVZs was explored, also using Spearman correlations, and compared with that of the above procedures to assess the specific vulnerability to nitrate pollution (Fig. 6; Table 8). No significant correlations were observed between the percent coverages of vulnerable areas (at high to extreme risk) extracted from the IV map and the IV' maps using the parameters S_{CH}, S_{St} + G + S and S_C (Fig. 5) and the percent coverages of the alluvial areas polluted by nitrates over the alluvial area. However, weak significant correlations were found against the percent coverages of alluvial areas polluted by nitrate over the catchment area, suggesting that the IV and IV' indices could have some utility in estimating NVZ (even though they were not specifically designed to assess vulnerability to nitrate pollution). The same was not observed for DRASTIC–COP. The percent coverages of vulnerable areas extracted from the DRASTIC–COP map (Fig. 5) against the percent coverages of the alluvial areas polluted by nitrates showed significant negative correlations (Table 9), revealing an unexpected inverse relationship between the areas defined as vulnerable and the areas polluted by nitrate in the experimental catchments. This anomalous result can be explained because the DRASTIC–COP map assessed as at medium risk a large part of the alluvial areas (Fig. 5), which were not included in the correlations. Correlations results from DRASTIC–COP became positive when the surface at medium to extreme risk was included as vulnerable areas in the analyses (Rho: 0.06, P-value: 0.91; and Rho: 0.23, P-value: 0.66), but no significant correlations were obtained. Nadiri et al. (2018c, 2019) and Hamamin and Nadiri (2018) improved the DRASTIC system using artificial intelligence or similar techniques to minimize uncertainty associated with its seven essential parameters and obtain more realistic results.

In light of the above results, the original LU–IV procedure (that uses readily available parameters) can be considered the best and simplest method of those tested in this study for delineating NVZs. So far, it has been applied in the Ebro River basin (Spain; tested and validated on 46 groundwater masses, of which 12 were alluvial aquifers; Arauzo, 2017; Arauzo et al., 2019, 2020), and the middle Nile River basin (Egypt;

Table 8

Validations of the six models to assess the specific vulnerability to nitrate pollution and estimate NVZs (Fig. 6). Validation based on Spearman correlations (Rho) between the percent coverage of NVZs (over the catchment area) vs the percent coverage of alluvial areas polluted by nitrate (over the total alluvial area and the catchment area). Datasets were extracted, catchment by catchment, from the experimental catchment areas C–1 to C–6 ($n = 6$).

Percent coverage of NVZs (% CA)	Percent coverage of alluvial areas polluted by nitrate over the alluvial area (%AA)		Percent coverage of alluvial areas polluted by nitrate over the catchment area (% CA)	
	Rho	P-value	Rho	P-value
Model 1: NVZs extracted from the original LU–IV procedure	0.93	0.008	0.99	0.0003
Model 2 (NEW): NVZs extracted from LU–IV' procedure using the parameter S _{HC}	0.93	0.008	0.99	0.0003
Model 3 (NEW): NVZs extracted from LU–IV' procedure using the parameter S _{St} + G + S	0.93	0.008	0.99	0.0003
Model 4 (NEW): NVZs extracted from LU–IV' procedure using the parameter S _C	0.93	0.008	0.99	0.0003
Model 5 (NEW): NVZs extracted from LU–DRASTIC–COP procedure	0.55	0.26	0.61	0.20
Model 6: Officially designated NVZ	0.51	0.30	0.69	0.13

Table 9

Validations of the five indices of intrinsic vulnerability (Fig. 5) as potential estimators of NVZs. Validation based on Spearman correlations (Rho) between the percent coverage of vulnerable areas extracted from each map of intrinsic vulnerability (over the catchment area) vs the percent coverage of alluvial areas polluted by nitrate (over the total alluvial area and the catchment area). Datasets were extracted, catchment by catchment, from the experimental catchment areas C-1 to C-6 ($n = 6$).

Percent coverage of vulnerable areas (% CA)	Percent coverage of alluvial areas polluted by nitrate over the alluvial area (%AA)		Percent coverage of alluvial areas polluted by nitrate over the catchment area (% CA)	
	Rho	P-value	Rho	P-value
Vulnerable areas extracted from the IV map	0.72	0.10	0.84	0.04
Vulnerable areas extracted from the IV' map using the parameter S _{HC}	0.58	0.23	0.75	0.08
Vulnerable areas extracted from the IV' map using the parameter S _{St} + G + S	0.58	0.23	0.75	0.08
Vulnerable areas extracted from the IV' map using the parameter S _C	0.58	0.23	0.75	0.08
Vulnerable areas extracted from the DRASTIC-COP map	-0.93	0.01	-0.87	0.02

Salman et al., 2019). The method should, however, be tested in more international studies.

NVZs estimated from the LU-IV procedure covered a surface area of 216 km² (15.4 % of the study area), which contrasts with the 94 km² officially designated as NVZ (6.7 % of the study area).

4. Conclusions

No significant recovery of groundwater quality has been observed in the Oja and Tirón alluvial aquifers since the 2006 NVZ designation, suggesting the need to review their NVZs.

Results of this investigation help refute the excessively simplistic idea that aquifer recharge is produced only by vertical infiltration, on which most methods for mapping groundwater vulnerability are based. As recharge can also come from places far away from the aquifer, groundwater vulnerability should be assessed in the entire catchment area of the aquifer, which is precisely one of the differential characteristics of the LU-IV procedure. The procedure is a novel method that combines a map of intrinsic vulnerability (based on the IV index) and a map of the risk of N-loss associated with land use (that uses the N-surpluses from the annual reports on N-balances in crops) to generate a map of vulnerability to nitrate pollution that covers the entire surface area of the territory. This methodology considers the importance of hydrology-controlled transport through catchment systems (an advance to solve the research gaps related to vulnerability assessment mapping), allowing a delineation of NVZs based on more realistic criteria.

In this research, it was analysed if NVZ delineation would be improved by introducing a new parameter representing the risk associated with soil permeability (parameter S) in the IV index of the LU-IV procedure. Different versions of parameter S were tested: parameter S_{HC} (risk associated with soil hydraulic conductivity), parameter S_{St} + G + S (risk associated with the stone, gravel and sand fraction of the soil) and parameter S_C (risk associated with the clay fraction). The efficacy of the following six models was tested and compared: Model 1 (original LU-IV procedure), Model 2 (LU-IV' procedure using parameter S_{HC}), Model 3 (LU-IV' procedure using parameter S_{St} + G + S), Model 4 (LU-IV' procedure using parameter S_C), Model 5 (LU-DRASTIC-COP procedure, based on the classical methods DRASTIC and COP), and Model 6 (officially designated NVZs). Statistical analyses on the intrinsic vulnerability maps of Models 1–4 showed that the inclusion of different versions of the parameter representing the risk associated with soil permeability in Models 2–4 (parameters S_{HC}, S_{St} + G + S and S_C) refined results compared to Model 1, but without any significant changes. This suggests that the inclusion of that parameter could be unnecessary. The intrinsic vulnerability map of Model 5 differed from those of the previous models, in part because it did not analyse the areas without underlying groundwater.

Unlike the DRASTIC index, the IV and IV' indexes for assessing intrinsic vulnerability assign the same theoretical weight to their parameters. Results of the single-parameter sensitivity analyses point to the convenience of not pre-assigning different weights to the input

parameters of the vulnerability indexes to minimize the impact of the subjective component linked to such pre-assignment. This helps explain the discrepancies between Models 1–4 and Model 5 in assessing intrinsic vulnerability.

Assessment of the specific vulnerability to nitrate pollution showed that the estimated NVZs from Models 1–4 covered most of the alluvial areas and their surrounding territories, under intensive agriculture, both in the Oja and Tirón aquifers. Models 5 and 6 covered smaller surfaces. Statistical analyses on the NVZ maps from the six models showed that Models 5 and 6, although statistically significant, presented weaker correlations with each other and with Models 1–4.

Catchment scale validations of the six vulnerability models showed similar, highly significant correlations between the percent coverages of the estimated NVZs and those of the alluvial areas polluted by nitrate for Models 1–4. Models 5 and 6 did not show any statistically significant results. In light of these results, Models 1–4 were considered the best predictors of nitrate pollution and the best methods for accurate NVZ delineation. These results support the idea that including a parameter representing the risk associated with soil permeability in the LU-IV' procedure of Models 2–4 is not essential since equivalent results were obtained from the original LU-IV procedure of Model 1. Therefore, the LU-IV procedure should be considered the best and simplest method of those tested to delimit NVZs.

CRediT authorship contribution statement

Mercedes Arauzo: Conceptualization, Methodology, Validation, Formal analysis, Investigation, Resources, Writing – original draft, Writing – review & editing, Visualization, Supervision, Project administration, Funding acquisition. **María Valladolid:** Methodology, Validation, Writing – review & editing, Visualization, Supervision. **Delia M. Andries:** Methodology, Validation, Writing – review & editing, Visualization, Supervision.

Declaration of competing interest

The authors declare that they have no known competing financial interests or personal relationships that could have appeared to influence the work reported in this paper.

Acknowledgements

The authors acknowledge the Spanish Ministry of Science and Innovation, the Spanish State Research Agency and the European Regional Development Fund for their financial support of Project CGL2016–81110–R (MCIN/AEI/FEDER, EU) and the Spanish Ministry of the Environment and Rural and Marine Affairs for providing the digital Crops and Land Use map of Spain. We also thank Marco Sagredo and Manuel Segura for their participation in the fieldwork, and Gema García, who coordinated the laboratory work.

References

- Aller, L., Bennet, T., Lehr, J.H., Petty, R.J., 1987. DRASTIC. A Standardized System for Evaluating Groundwater Pollution Potential Using Hydrogeologic Settings (U.S. EPA Report 600/2-87-035, Oklahoma).
- Arauzo, M., 2017. Vulnerability of groundwater resources to nitrate pollution: a simple and effective procedure for delimiting nitrate vulnerable zones. *Sci. Total Environ.* 575, 799–812. <https://doi.org/10.1016/j.scitotenv.2016.09.139>.
- Arauzo, M., Martínez-Bastida, J.J., 2015. Environmental factors affecting diffuse nitrate pollution in the major aquifers of Central Spain: groundwater vulnerability vs. Groundwater pollution. *Environ. Earth Sci.* 73, 8272–8286. <https://doi.org/10.1007/s12665-014-3989-8>.
- Arauzo, M., Valladolid, M., 2013. Drainage and N-leaching in alluvial soils under agricultural land uses: implications for the implementation of the EU nitrates directive. *Agric. Ecosyst. Environ.* 179, 94–107. <https://doi.org/10.1016/j.agee.2013.07.013>.
- Arauzo, M., Valladolid, M., Martínez-Bastida, J.J., 2011. Spatio-temporal dynamics of nitrogen in river-alluvial aquifer systems affected by diffuse pollution from agricultural sources: implications for the implementation of the nitrate directive. *J. Hydrol.* 411, 155–168. <https://doi.org/10.1016/j.jhydrol.2011.10.004>.
- Arauzo, M., García, G., Valladolid, M., 2019. Assessment of the risks of N-loss to groundwater from data on N-balance surplus in Spanish crops: an empirical basis to identify nitrate vulnerable zones. *Sci. Total Environ.* 696, 133713. <https://doi.org/10.1016/j.scitotenv.2019.133713>.
- Arauzo, M., Valladolid, M., García, G., 2020. Mapping groundwater vulnerability to nitrate pollution from diffuse sources in the Ebro River basin (N.E. Spain) (Cartografía de la vulnerabilidad de las aguas subterráneas a la contaminación por nitratos de Fuentes difusas en la Cuenca del río Ebro (N.E. de España); Spanish). *Estud. Geol.* 76, e132. <https://doi.org/10.3989/egool.43868.586>.
- Arauzo, M., Valladolid, M., García, G., Andries, D.M., 2022. N and P behaviour in alluvial aquifers and in the soil solution of their catchment areas: how land use and the physical environment contribute to diffuse pollution. *Sci. Total Environ.* 804, 150056. <https://doi.org/10.1016/j.scitotenv.2021.150056>.
- Arqued, V.M., 2018. It is likely that the areas designated as nitrate vulnerable zones will be expanded (Es probable que se amplíen las zonas declaradas Como vulnerables por la contaminación con nitratos agrícolas; Spanish). *Tierras Agric.* 268, 120–122.
- Babiker, I.S., Mohamed, M.A., Hiyama, T., Kato, K., 2005. A GIS-based DRASTIC model for assessing aquifer vulnerability in Kakamigahara Heights, Gifu prefecture, Central Japan. *Sci. Total Environ.* 345, 127–140. <https://doi.org/10.1016/j.scitotenv.2004.11.005>.
- Bear, J., 1972. *Dynamic of Fluids in Porous Media*. Dover Publications, Inc., New York.
- Botey, R., Guijarro, J.A., Jiménez, A., 2013. Normal monthly precipitation from 1981–2010 (Valores normales de precipitación mensual 1981–2010; Spanish). Dirección de Producción e Infraestructuras, Agencia Estatal de Meteorología (AEMET), Ministerio de Agricultura, Alimentación y Medio Ambiente, Madrid.
- Boy-Roura, M., Nolan, B.T., Menció, A., Mas-Pla, J., 2013. Regression model for aquifer vulnerability assessment of nitrate pollution in the Osona region (NE Spain). *J. Hydrol.* 505, 150–162. <https://doi.org/10.1016/j.jhydrol.2013.09.048>.
- Council of the European Communities, 1991. Directive 91/676/EEC concerning the protection of waters against pollution caused by nitrates from agricultural sources. 12 December 1991. *Official Journal of the European Union L 375* 31/12/1991, Brussels.
- Debernardi, L., De Luca, D.A., Lasagna, M., 2008. Correlation between nitrate concentration in groundwater and parameters affecting aquifer intrinsic vulnerability. *Environ. Geol.* 55, 539–558. <https://doi.org/10.1007/s00254-007-1006-1>.
- Decagon Devices Inc., 2016. Mini disk infiltrometer manual, Ver. September 2, 2016. Decagon Devices Inc., Pullman, WA. http://manuals.decagon.com/Manuals/10564_MiniDiskInfiltrometer_Print.pdf. (Accessed 14 December 2021).
- ESRI, 2015. ArcGIS Desktop: Release 10.3. Environmental Systems Research Institute, Redlands, CA.
- European Commission, 2018. Report from the Commission to the Council and the European Parliament on the implementation of Council Directive 91/676/EEC concerning the protection of waters against pollution caused by nitrates from agricultural sources based on Member State reports for the period 2012–2015. 52010DC0047-EUR-Lex, Brussels. https://ec.europa.eu/environment/water/water-nitrates/pdf/nitrates_directive_implementation_report.pdf. (Accessed 10 August 2021).
- Everst, C.J., Kanwar, R.S., 1993. Interpreting tension-infiltration data for quantifying soil macropores: some practical considerations. *Trans. ASAE* 36, 423–428. <https://doi.org/10.13031/2013.28354>.
- FAO, 2021. Soil Permeability (Chapter 9). Soil. FAO Training Series. http://www.fao.org/fishery/docs/CDrom/FAO_Training/FAO_Training/General/x6706e/Index.htm. (Accessed 15 September 2021).
- Fortaleza, J., Lorenzo, L.F., Najac, N., Cuadrado, S., Ingelmo, F., Hernández, J., García, M.P., Prat, L., Muñoz, M.C., Macarro, M.C., Rivas, M.D., 1987. Soil Map of Castilla y León (Mapa de Suelos de Castilla y León; Spanish). 1:500,000. Junta de Castilla y León, León.
- Foster, S.S.D., Hirata, R., Gómez, D., D'Elia, M., Paris, M., 2002. Ground water Quality Protection. A guide for water utilities, municipal authorities and environment agencies. The World Bank, Washington D.C. <http://hdl.handle.net/10986/13843>. (Accessed 4 September 2015).
- Franceys, R., Pickford, J., Reed, R., 1992. A guide to the development of on-site sanitation. World Health Organization. <https://apps.who.int/iris/handle/10665/39313>. (Accessed 7 July 2021).
- Gobierno de la Rioja, 2006. Decree 12/2006 (Decreto 12/2006; Spanish). Consejería de Agricultura y Desarrollo Económico. Boletín Oficial de La Rioja. 19, p. 720.
- Gobierno de la Rioja, 2006. Map of agricultural soils of La Rioja, scale 1:100,000, version 1.1, ref. study: SUE-1-05 (Mapa de suelos agrícolas de La Rioja, escala 1:100.000, versión 1.1, ref. estudio: SUE-1-05; Spanish). Agrogeotec. Consejería de Agricultura y Desarrollo Económico, Gobierno de La Rioja. Logroño.
- Gobierno de la Rioja, 2010. Master plan for wastewater sanitation and treatment of La Rioja (Plan director de saneamiento y depuración de La Rioja; Spanish). Consejería de Turismo, Medio Ambiente y Política Territorial, Dirección General del Agua, Logroño.
- Guerra, A., Monturiol, F., Badorey, T., Gallardo, J., Carlevaris, J.J., de la Horra, J.L., Labrander, J.L., 1970. Soil Map of the Provinces of Zaragoza, Huesca and Logroño (Mapa de suelos de las provincias de Zaragoza, Huesca y Logroño; Spanish). 1: 250,000. Instituto Nacional de Edafología y Agrobiología José María Albareda, CSIC, Madrid.
- Hamamin, D.F., Nadiri, A.A., 2018. Supervised committee fuzzy logic model to assess groundwater intrinsic vulnerability in multiple aquifer systems. *Arab. J. Geosci.* 11, 176. <https://doi.org/10.1007/s12517-018-3517-3>.
- Hamza, S.M., Ahsan, A., Imteaz, M.A., Rahman, A., Mohammad, T.A., Ghazali, A.H., 2015. Accomplishment and subjectivity of GIS-based DRASTIC groundwater vulnerability assessment method: a review. *Environ. Earth Sci.* 73, 3063–3076. <https://doi.org/10.1007/s12665-014-3601-2>.
- Hrachowitz, M., Benettin, P., Breukelen, B.M., Fovet, O., Howden, N.J.K., Ruiz, L., Velde, Y., Wade, A.J., 2016. Transit times –the link between hydrology and water quality at the catchment scale. *WIREs Water* 3, 629–657. <https://doi.org/10.1002/wat2.1155>.
- IBM Corp. Released, 2020. IBM SPSS Statistics for Windows, Version 27.0. IBM Corp., Armonk, NY.
- IGME, 2009. Map of groundwater vulnerability to pollution. Reduced version of the DRASTIC index. Ebro River basin. Assessment of the intrinsic vulnerability of intercommunity groundwater. Detrital and mixed masses (Mapa de vulnerabilidad a la contaminación del agua subterránea. Índice DRASTIC reducido. Demarcación Hidrográfica del Ebro. Evaluación de la vulnerabilidad intrínseca de las aguas subterráneas intercomunitarias. Masas detriticas y mixtas; Spanish) [map in digital format]. 1:1,000,000. Instituto Geológico y Minero de España, Dirección General del Agua. <http://www.igme.es/>. (Accessed 6 February 2016).
- IGME, 2009. Map of groundwater vulnerability to pollution. COP method. Ebro River basin. Assessment of the intrinsic vulnerability of intercommunity groundwater. Carbonated masses (Mapa de vulnerabilidad a la contaminación del agua subterránea. Método COP. Demarcación Hidrográfica del Ebro. Evaluación de la vulnerabilidad intrínseca de las aguas subterráneas intercomunitarias. Masas carbonatadas; Spanish) [map in digital format]. 1:1,000,000. Instituto Geológico y Minero de España, Dirección General del Agua. <http://www.igme.es/>. (Accessed 6 February 2016).
- IGME, 2015. Geological map of Spain, MAGNA Series; Geological and Mining Institute of Spain (Mapa geológico de España, Series MAGNA; Instituto Geológico y Minero de España; Spanish) [maps in digital format]. 1:50,000. <http://iber.chebro.es/geoportal/>. (Accessed 12 October 2015).
- Javadi, S., Kavehkar, N., Mohammadi, K., Khodadadi, A., Kahawita, R., 2011. Calibrating DRASTIC using field measurements, sensitivity analysis and statistical methods to assess groundwater vulnerability. *Water Int.* 36, 719–732. <https://doi.org/10.1080/02508060.2011.610921>.
- Kumar, P., Bansod, B.K.S., Debnath, S.K., Kumar Thakur, P., Ghanshyam, C., 2015. Index-based groundwater vulnerability mapping models using hydrogeological settings: a critical evaluation. *Environ. Impact Assess. Rev.* 51, 38–49. <https://doi.org/10.1016/j.eiar.2015.02.001>.
- Kura, N.U., Ramli, M.F., Ibrahim, S., Sulaiman, W.N.A., Aris, A.Z., Tanko, A.I., Zaudi, M.A., 2015. Assessment of groundwater vulnerability to anthropogenic pollution and seawater intrusion in a small tropical island using index-based methods. *Environ. Sci. Pollut. Res.* 22, 1512–1533. <https://doi.org/10.1007/s11356-014-3444-0>.
- Machiwal, D., Jha, M.K., Singh, V.P., Mohan, C., 2018. Assessment and mapping of groundwater vulnerability to pollution: current status and challenges. *Earth-Sci. Rev.* 185, 901–927. <https://doi.org/10.1016/j.earscirev.2018.08.009>.
- MAPAMA, 2017. Nitrogen Balance in Spanish Agriculture for the Year 2015 (Balance del nitrógeno en la agricultura española, año 2015; Spanish). Ministerio de Agricultura y Pesca, Alimentación y Medio Ambiente, Secretaría General Agricultura y Alimentación, Dirección General de Producciones y Mercados Agrarios, Madrid.
- MAPAMA, 2018. Nitrogen Balance in Spanish Agriculture for the Year 2016 (Balance del nitrógeno en la agricultura española, año 2016; Spanish). Ministerio de Agricultura y Pesca, Alimentación y Medio Ambiente, Secretaría General Agricultura y Alimentación, Dirección General de Producciones y Mercados Agrarios, Madrid.
- MARM, 2009. Crops and Land Use Map of Spain 2000–09 (Mapa de Cultivos y Aprovechamientos de España 2000–09; Spanish) [Maps in Digital Format]. 1:50,000. Ministerio de Medio Ambiente, Medio Rural y Marino de España, Madrid.
- Martínez-Bastida, J.J., Arauzo, M., Valladolid, M., 2010. Intrinsic and specific vulnerability of groundwater in Central Spain: the risk of nitrate pollution. *Hydrogeol. J.* 18, 681–698. <https://doi.org/10.1007/s10040-009-0549-5>.
- Nadiri, A.A., Aghdam, F.S., Khatibi, R., Moghaddam, A.A., 2018a. The problem of identifying arsenic anomalies in the basin of Sahand dam through risk-based 'soft modelling'. *Sci. Total Environ.* 613–614, 693–706. <https://doi.org/10.1016/j.scitotenv.2017.08.027>.
- Nadiri, A.A., Sadeghfar, S., Gharekhani, M., Khatibi, R., Akbari, B., 2018b. Introducing the risk aggregation problem to aquifers exposed to impacts of anthropogenic and geogenic origins on a modular basis using 'risk cells'. *J. Environ. Manag.* 217, 654–667. <https://doi.org/10.1016/j.jenvman.2018.04.011>.
- Nadiri, A.A., Sedghi, Z., Khatibi, R., Sadeghfar, S., 2018c. Mapping specific vulnerability of multiple confined and unconfined aquifers by using artificial intelligence to learn from multiple DRASTIC frameworks. *J. Environ. Manag.* 227, 415–428. <https://doi.org/10.1016/j.jenvman.2018.08.019>.
- Nadiri, A.A., Norouzi, H., Khatibi, R., Gharekhani, M., 2019. Groundwater DRASTIC vulnerability mapping by unsupervised and supervised techniques using a modelling strategy in two levels. *J. Hydrol.* 574, 744–759. <https://doi.org/10.1016/j.jhydrol.2019.04.039>.
- Orellana-Macias, J.M., Merchán, D., Causapé, J., 2020. Evolution and assessment of a nitrate vulnerable zone over 20 years: Gallocañta groundwater body (Spain). *Hydrogeol. J.* 28, 2207–2221. <https://doi.org/10.1007/s10040-020-02184-0>.

- Richard, A., Casagrande, M., Jeuffroy, M.H., David, C., 2018. An innovative method to assess suitability of nitrate directive measures for farm management. *Land Use Policy* 72, 389–401. <https://doi.org/10.1016/j.landusepol.2017.12.059>.
- Salman, A.A., Arauzo, M., Elnazer, A.A., 2019. Groundwater quality and vulnerability assessment in west Luxor Governorate, Egypt. *Groundw. Sustain. Development* 8, 271–280. <https://doi.org/10.1016/j.gsd.2018.11.009>.
- Stigter, T.Y., Ribeiro, L., Carvalho Dill, A.M.M., 2006. Evaluation of an intrinsic and a specific vulnerability assessment method in comparison with groundwater salinisation and nitrate contamination levels in two agricultural regions in the south of Portugal. *Hydrogeol. J.* 14, 79–99. <https://doi.org/10.1007/s10040-004-0396-3>.
- USDA, 2021. Saturated hydraulic conductivity: water movement concepts and class history. Natural Resources Conservation Service. Soils. United States Department of Agriculture. https://www.nrcs.usda.gov/wps/portal/nrcs/detail/soils/ref/?cid=nrcs142p2_053573. (Accessed 15 September 2021).
- Vías, J.M., Andreo, B., Perles, M.J., Carrasco, F., Vadillo, I., Jiménez, P., 2006. Proposed method for groundwater vulnerability mapping in carbonate (karstic) aquifers: the COP method. *Hydrogeol. J.* 14, 912–925. <https://doi.org/10.1007/s10040-006-0023-6>.
- Groundwater vulnerability assessment and mapping. In: Witkowski, A., Kowalczyk, A., Vrba, J. (Eds.), *IAH-selected Papers*. 11. Taylor & Francis, London.
- Worrall, F., Spencer, E., Burt, T.P., 2009. The effectiveness of nitrate vulnerable zones for limiting surface water nitrate concentrations. *J. Hydrol.* 370, 21–28. <https://doi.org/10.1016/j.jhydrol.2009.02.036>.
- Zahid, A., Hassan, M.Q., Ahmed, K.M.U., 2015. Simulation of flowpaths and travel time of groundwater through arsenic-contaminated zone in the multi-layered aquifer system of Bengal Basin. *Environ. Earth Sci.* 73, 979–991. <https://doi.org/10.1007/s12665-014-3447-7>.